

**THE STUDY OF A SOLAR ASSISTED HEAT PUMP
DESALINATION SYSTEM**

**By:
Tobias Bestari Tjandra (B.Eng)
HT050297H**

**A THESIS SUBMITTED FOR THE DEGREE OF
MASTER OF ENGINEERING**

**Department of Mechanical Engineering
National University of Singapore
2007**

SUMMARY

Located at the equator (1°21'N; 103°55'E), Singapore has abundant solar radiation and high ambient temperature throughout the year. Singapore's meteorological data indicate favorable conditions for the efficient operation of solar energy systems. To study the performance of a desalination system, experiments were conducted on a solar assisted heat pump desalination system at the National University of Singapore.

The system consists of two modules, a solar assisted heat pump and a water distillation unit. The main components of the solar assisted heat pump consist of an unglazed, serpentine-tube evaporator-collector, a compressor, a water condenser tank, and an expansion valve. The water distillation unit consists of a glazed liquid solar collector, an electrical heater, and a distillation chamber. A condenser coil is located at the bottom of the chamber to evaporate saturated water, and a cooling coil is located at the top section of the chamber to condense vapors. These coils are connected to the condenser and evaporator section of the heat pump. Refrigerant R134a was used as the working fluid for the heat pump. The distillation chamber was operated at 0.14 bar, which corresponds to water saturation temperature of 52 °C. The liquid solar collector and electrical heater will heat the feed water until it reaches 70 °C. Upon entering the distillation chamber feed water undergoes thermodynamic flashing. Saturated water will then be evaporated further by condenser coils of the heat pump system. Vapors from flashing and evaporation are then condensed by a cooling coil located in the top section of the chamber, thus producing fresh water.

A series of experiments have been conducted with the system under the meteorological conditions of Singapore. Experiments were carried out to find the efficiencies of evaporator-collector and liquid collector, Coefficient of Performance (COP) of the heat pump system, distillate produced, and Performance Ratio (PR). Mathematical equations were developed for each component of the system, and a simulation program was then written. Comparison of the simulation and experimental results showed good agreement. To further analyze the behavior of the system, a parametric study was conducted, followed by an economic optimization.

Results showed that the system has a Coefficient of Performance that is close to 10, with collector efficiencies between 80 to 90 % and 50 to 60 % for evaporator-collector and liquid collector, respectively. The system has a Performance Ratio close to 1.5, with a water production rate close to 1 kg/hr. Economic analyses showed that for the system to be economically feasible, its production rate needs to be increased, while keeping the investment cost as low as possible. To achieve this goal, a new design of the system was proposed. To reduce the investment cost of the system, the new design leaves out the use of a liquid solar collector. This way the investment cost is kept low, and the system may achieve a payback period close to 3.5 years with a production rate of 900 l/day. To achieve this condition, the evaporator collector area will need to be around 70 m², and 30 kW is needed for compressor work. Further analyses of economic parameters showed that fuel price will determine the feasibility of the solar desalination system. The study showed that solar energy is a very promising source of thermal energy to be applied in desalination processes. With the rising price of oil, solar energy becomes economically competitive. Further studies will be needed to fully exploit the use of solar energy in desalination systems.

ACKNOWLEDGEMENTS

The author would like to express his gratitude to A/Prof. M.N.A. Hawlader for his support, advice, and guidance during the author's course of study for the M. Eng degree.

The author would also like to extend his appreciation to the following persons for their assistance and support:

Mr Jahangeer s/o Abdul Rahman, Mr Ling Moh Lung, Mr Suratin bin Suwandi, and Mr. Ng Jun Lin, who provided help and advice in this project.

I would also like to thank my friends in the Energy Conversion Lab, Thermal Process Lab 1 and 2: Mr Tan Tiong Thiam, Mr S.M. Atiqure Rahman, Ms Papia Sultana, Mr Wang Shi Jun, Mr Fazole Mahbub, Mr Yeo Khee Ho, Mr Chew Yew Lin, Mr Anwar Sadat, and Ms Roslina Abdullah.

I am deeply grateful for my close friends: Mr Agus Pulung Sasmito, Mr Tandiono Tan, Ms Filian Arbiyani, and Mr Andreas Lo, who provided the support and inspiration which enabled the conclusion of the project successfully.

And last but not the least, I thank my parents and friends who are not mentioned above, and especially Ms Khoo Fuk Ling for their love, encouragement, and understanding.

Table of Contents

Summary	i
Acknowledgements	iii
Table of Contents	iv
List of Figures	vii
List of Tables	ix
List of Symbols	x
Chapter 1 Introduction	1
1.1. Background	1
1.2. Objectives of Research	3
1.3. Scope of the Thesis	3
Chapter 2 Literature Review	5
2.1. Thermal Desalination Processes	6
2.2. Solar Energy and Heat Pump Desalination Processes	7
2.3. Economic Analysis of Solar Energy Processes	14
Chapter 3 Experiments	17
3.1. Working Principle of the SAHPD	17
3.2. Components of the system	19
3.2.1. Evaporator collector	19
3.2.2 Liquid collector	19

3.2.3. Compressor	20
3.2.4. Thermostatic expansion valve	21
3.2.5. Water condenser tank	21
3.2.6. Desalination chamber	22
3.2.7. Electrical heater	23
3.2.8. Pumps	23
3.3. Instrumentation	23
3.4. Procedure of Experiment	25
Chapter 4 Modeling, Simulation, and Optimization	27
4.1. Modeling of Components	27
4.1.1. Liquid solar collector	27
4.1.2. Evaporator Collector	31
4.1.2.1. Pressure drop in evaporator collector	32
4.1.3. Desalination chamber	33
4.1.4. Compressor model	37
4.1.5. Condenser model	38
4.1.6. Thermostatic expansion valve	39
4.1.7. Electric heater	39
4.1.8. Performance parameters	39
4.2. Meteorological Data of Singapore	40
4.2.1. Singapore's Climatic Conditions	41
4.2.2. Correlation for Singapore's Meteorological Conditions	41
4.3. Simulation Algorithm	43

4.4. Economic Optimization	48
4.4.1. Annualized cost	49
4.4.2. Life Cycle Savings	50
4.4.3. Payback Period	50
Chapter 5 Results and Discussion	51
5.1. Meteorological Condition of Singapore	51
5.2. Experimental Results	52
5.3. Comparison of Experimental and Simulation Results	60
5.4. Results of Parametric Study	63
5.5. Results of economic optimization	68
Chapter 6 Conclusions	77
Chapter 7 Recommendations	79
References	80
Appendix A Experimental Data	83
Appendix B Compressor Price List and Air Conditioner Cooling Capacity	93
Appendix C Sample Calculation	96

LIST OF FIGURES

Figure 3.1. Solar assisted heat pump desalination system setup	18
Figure 3.2. Schematic of evaporator and water solar collector	19
Figure 3.3. Compressor	20
Figure 3.4. Frequency inverter	20
Figure 3.5. Thermostatic expansion valve	21
Figure 3.6. Water condenser tank	21
Figure 3.7. Desalination chamber	22
Figure 4.1. Cross section of solar collector	30
Figure 4.2. Heat transfer processes taking place inside the desalination chamber	34
Figure 4.3. Cross section of heat exchanger tube	36
Figure 4.4. Flowchart of the simulation program	46
Figure 4.5. Flowchart of evaporator collector	47
Figure 5.1. Values for solar radiation and ambient temperature in January 2006	52
Figure 5.2. Values for relative humidity and wind speed in January 2006	52
Figure 5.3. Change of evaporator collector efficiency and solar radiation with time	53
Figure 5.4. Change of evaporator collector efficiency and ambient temperature with time	54
Figure 5.5. Change of liquid collector efficiency and solar radiation with time	54
Figure 5.6. Liquid solar collector efficiency as a function of water inlet temperature and solar radiation	55
Figure 5.7. Evaporator collector efficiency as a function of refrigerant inlet temperature and solar radiation	55
Figure 5.8. Change of COP and solar radiation with time	56
Figure 5.9. Change of COP and ambient temperature with time	56

Figure 5.10. Water production rate and performance ratio	57
Figure 5.11. Comparison of water production rate and average solar radiation	58
Figure 5.12. The change of COP to Solar radiation	59
Figure 5.13 The effect of solar radiation to production rate	59
Figure 5.14. Solar radiation and ambient temperature for a day in December	60
Figure 5.15 Comparison of simulated and experimental result of liquid collector efficiency	61
Figure 5.16 Comparison of simulated and experimental result of evaporator collector efficiency	61
Figure 5.17 Comparison of simulated and experimental result of COP	62
Figure 5.18 Comparison of simulated and experimental result of water production	62
Figure 5.19 Comparison of simulated and experimental result of Performance Ratio	63
Figure 5.20 Effect of feed temperature to production rate and liquid collector area	64
Figure 5.21 Effects of solar radiation on production rate and liquid collector efficiency	65
Figure 5.22 Effect of ambient temperature to production rate and feed temperature ($I = 600 \text{ W/m}^2$, chamber pressure at 0.14 bar)	66
Figure 5.23 Effect of chamber pressure to production rate	66
Figure 5.24 Effect of solar radiation to evaporator outlet temperature and production rate	67
Figure 5.25. Effect of compressor running frequency to production rate and electricity consumption	67
Figure 5.26 Proposed solar heat pump desalination setup	71
Figure 5.27 Comparison of payback period for different production rates	72
Figure 5.28 Comparison of payback period with the usage of liquid solar collector	72
Figure 5.29 Effect of discount rate (Production rate: 900 l/day)	73
Figure 5.30 Effect of inflation rate (Production rate: 900 l/day)	74
Figure 5.31 Effect of fuel escalation rate (Production rate: 900 l/day)	75
Figure 5.32 Effect of fuel price (Production rate: 900 l/day)	75

LIST OF TABLES

Table 1.1. Population (thousands) and yearly water availability (m ³ /capita) in the South Mediterranean [Fiorenza et al., 2003]	1
Table 2.1. Types of desalination processes	5
Table 3.1. Summary of main components	24
Table 4.1. Solar radiation coefficients	42
Table 4.2. Temperature coefficients	42
Table 4.3. Wind speed coefficients	43
Table 5.1 Parameters used in economic figures	69
Table 5.2 Water requirement of commercial and institutional buildings [Stein et al, 1986]	70
Table A1. Experimental data of 12 December 2005	83
Table A2. Experimental data for 13 December 2005	86
Table A3. Experimental data for 23 January 2006	89
Table B1. Compressor prices (www.thermacom.com)	93
Table B2. Cooling capacity of air conditioners (www.daikin.com.sg)	94

LIST OF SYMBOLS

Modelling of components

A_C	Collector area, m ²
b	Collector bond width, m
C	Compressor clearance volumetric ratio
$c_{p,w}$	Specific heat of water, kJ/kg K
C_b	Collector bond conductance, kW/m K
D_o	Tube outer diameter, m
D_i	Tube inner diameter, m
ε	Error margin
F	Collector fin efficiency ratio
F'	Collector efficiency factor
F_R	Collector heat removal factor
h_W	Wind heat transfer coefficient, W/m ² K
$h_{f,i}$	Fluid heat transfer coefficient, W/m ² K
h_{fg}	Latent heat of vaporization, kJ/kg
I	Solar irradiation, W/m ²
k_b	Collector bond thermal conductivity, kW/m K
μ	Fluid dynamic viscosity, kg/m s
\dot{m}_w	Mass flow rate of water, kg/s
\dot{m}_{ref}	Mass flow rate of refrigerant, kg/s

Q_u	Useful energy gained by collector, W
ρ	Density of fluid, kg/m ³
σ	Stefan Boltzmann coefficient, $5.67 \cdot 10^{-8}$ W/m ² K ⁴
T_w	Temperature of water, K
T_a	Temperature of Ambient, K
$T_{p,m}$	Plate mean temperature, K
$\tau\alpha$	Transmissivity-absorptivity product
U_t	Collector top loss coefficient
U_L	Collector overall loss coefficient
U_b	Collector bottom loss coefficient

Economic parameters

C_F	Fuel price, S\$/MJ
C_M	Maintenance cost, S\$
C_O	Operation cost, S\$
C_{RF}	Capital recovery factor
C_s	Collector investment cost, S\$
e	Fuel escalation rate
i	Discount rate
n	System life cycle, years
Q_s	Solar energy input, MJ

Chapter 1

INTRODUCTION

1.1. Background

It is a well known fact that water is the most important element in life. All living beings need water to continue on living. Mankind need water to maintain life, perform domestic tasks, and maintain industry. However, recent research shown that around 25% of the world population does not have an adequate supply of fresh water, both in terms quality and quantity. This tragic situation has been in place for nearly 80 countries, and demands very urgent attention. [Fiorenza et al., 2003]

The world population, numbering a little more than 6 billion, may touch an unimaginable Figure of nearly 8 and 9 billion during the year 2025 and 2050 [Fiorenza et al., 2003]. This increase in population will mostly take place in developing countries, causing severe water shortages. By the year 2020, water availability will be less than the minimum level recommended by the World Health Organization (WHO). The situation will be worse, with an annual availability of less than 200 m³ per capita, in the majority of countries listed in Table 1.1.

Table 1.1. Population (thousands) and yearly water availability (m³/capita) in the South Mediterranean [Fiorenza et al., 2003]

Country	Population			Water availability (m ³ /capita)		
	1960	1990	2020	1960	1990	2020
Saudi Arabia	4,075,000	16,045,000	36,424,000	537	156	54
Libya	1,349,000	4,416,000	8,103,000	538	154	59
Malta	312,000	354,000	427,000	100	75	76
Yemen	5,247,000	11,590,000	34,190,000	481	214	82
Jordan	763,000	3,306,000	8,204,000	529	224	100
United Arab Emirates	90,000	1,921,000	3,170,000	3,000	189	117

Table 1.1. (Continued)

Syria	4,561,000	12,386,000	24,555,000	1,196	439	172
Israel	2,114,000	4,660,000	7,952,000	1,024	467	324
Tunisia	4,221,000	8,156,000	12,254,000	1,036	532	334
Algeria	10,800,000	24,936,000	43,853,000	1,704	737	376
Oman	558,000	1,785,000	4,719,000	4,000	1,333	477
Egypt	27,840,000	56,333,000	90,491,000	2,251	1,112	682
Morocco	11,626,000	23,931,000	36,742,000	2,650	1,185	685

Although 75% of the earth's surface is covered by water, 97.5% of this abundant source of water is salty, while the remaining part is mostly in a frozen form, or located deep underground, virtually inaccessible. It is, therefore, obvious that the sea is basically an easily accessible source of water, as long as its salinity can be removed.

As a source of water, seawater has a salinity in the range of 35,000-45,000 parts per million (ppm), much higher than the permissible limit of 500 ppm according to the World Health Organization [Kalogirou, 2005].

Desalination is basically a process to remove salt from seawater or saline water. The purpose is to purify water, and produce potable water with dissolved solids within the permissible limit of 500 ppm. There are many methods of desalination. Nowadays, Multi Effect Distillation (MED) and Multi Stage Flash (MSF) are the two methods commonly used in desalination. However, these two processes require a large amount of thermal energy. The consumption of oil to generate the required heat will be very harmful to the environment. Therefore, it will be advantageous to implement a new and clean source of thermal energy. Solar energy fulfills this requirement.

Solar desalination is a desalination method involving solar energy in the process. Other than using solar energy, Reali, [1984], Slesarenko, [1999] have discussed about using heat pumps to provide heat in desalination processes.

In order to further investigate the potential of using solar energy and heat pumps for desalination processes, an experimental solar assisted-heat pump desalination system has been built at the National University of Singapore (NUS).

1.2. Objectives of Research

The main objective of this research can be described as follows:

- To perform experiments to identify important variables that affects the performance of the system.
- To develop a mathematical model and a simulation program based on the experimental system.
- To validate the results of the simulation with experimental results.
- To conduct a parametric study based on the simulation program.
- To conduct an economic analysis based on the system's performance and simulation results.

1.3. Scope of the Thesis

The thesis is divided into different sections and the order of presentation is as follows:

- Chapter 1 gives a brief background on the world's water condition, and also the objectives and scope of the project.
- Chapter 2 presents a literature review based on scientific journals and reports.

- Chapter 3 includes a description of the system and its working principle, its components, and the experimental procedure.
- Chapter 4 contains the mathematical model of the system, the algorithm of the simulation program and equations for economic optimization.
- Chapter 5 presents the results of the experiments, simulation program and economic optimization.
- Chapter 6 contains the conclusion of the work that has been carried out.
- Chapter 7 presents recommendations for future work.

Chapter 2

LITERATURE REVIEW

The desalination process has been known since ancient times, but perhaps the earliest known seawater desalination process took place in AD 200, where Greek sailors, in their long distance trips would boil seawater in a brass vessel and suspend large sponges on top of it to absorb the vapors. The water extracted from the sponge is found to be potable. [Kalogirou, 2005]

Nowadays there are many methods of desalination, however all methods require a pre-treatment of raw seawater to avoid scaling, foaming, corrosion, biological growth, and fouling. Shown in table 2.1, Khan [1986] divided the process into several categories, viewed from water's change of phase, utilization of energy, and separation of salt and water in the solution.

Table 2.1. Types of desalination processes

Desalination processes	
Thermal processes	Membrane processes
Multi Stage Flash (MSF) Multi Effect Distillation (MED) Vapor Compression (VC) Freezing Humidification/dehumidification Adsorption desalination Solar stills	Reverse Osmosis (RO) Electrodialysis (ED)

The most dominant commercial processes are MSF, MED, VC, and RO. Among these processes, MSF is the most popular of thermal processes and RO is the most popular of membrane processes.

2.1. Thermal Desalination Processes

Multi-stage flash desalination (MSF) is currently the most popular method in the desalination industry with a market share close to 60% of the total world production capacity. The process has several advantages, which include a large operation capacity, proven reliability, and well-developed construction and operation experience. El-Dessouky et al. [1999] conducted a study to observe the present and future outlook of the MSF process. In the study, they also proposed a novel configuration of the MSF system. With the new system, though depends on the temperature of the feed seawater, the salinity of the rejected brine can be less than the limiting value of 70,000 ppm. The new system has similar variations in thermal performance with the conventional MSF system, and gives higher thermal performance ratios with values ranging between 12 and 20.

Experiments using mechanical vapor compression system using two vertical evaporator-condensers were conducted by Bahar et al. [2004] The system has a production capacity of 1 m³/day. The experiments were conducted with variation in compressor speed and brine concentration, ranging from 20,000 ppm to 33,000 ppm. The highest performance ratio obtained was 2.52, and it was found out that an increase of the compressor speed had a positive influence on the system's performance..

Dvornikov [2000] conducted a feasibility study of a combined power and desalination plant incorporating horizontal falling film-type low temperature multi effect distiller (MED), Heat Recovery Steam Generator (HRSG), and a gas turbine, fueled by natural gas. The under study was based on a single shaft gas turbine of 38.3 MWe generating 139 kg/s

of hot flue gases at 545 °C. The MED system had a production capacity of 8760 ton of water per day, consuming 430 kW of electrical energy. The combination of the power and desalination plant proves to be a viable alternative for mid-size cogeneration projects with a variable power load and a uniform water demand.

Marcovecchio et al. [2005] proposed a hybrid MSF-RO system. The system aims to reduce operation and maintenance costs of the product water with an overall increase in recovery and reduction of energy consumption. From the study, it is found that the proposed system could produce 2500 ton of water per hour, with an optimal cost for water production of \$1.259/m³.

Wang and Ng (2005) conducted an experimental study with a four bed-silica gel adsorption desalination system. Compared to other desalination methods, the adsorption has several advantages such as: The utilization of the low-temperature waste heat, low corrosion and fouling rates on the tube materials due to the low temperature evaporation of saline water, and it has almost no major moving parts which renders inherently low maintenance cost. From the study, it was found that system has an optimum daily water production of 4.7 kg/kg silica gel.

2.2. Solar Energy and Heat Pump Desalination Processes

Experimental work on heat pump assisted water purification has been carried out in Mexico since 1981 by Siqueiros et al. [2000]. The heat pumps used were initially of the mechanical vapor compression type, which were later replaced by absorption heat pumps. They concluded that, from a thermodynamic point of view, it is much more appropriate to

use waste heat to operate water purification systems than using high grade energy such as electricity, oil, or natural gas with its associated environmental problems. The purification unit was designed to operate as a small scale mobile unit, able to provide potable water in disaster areas. Slesarenko [1999] investigated the application of the absorption heat pump in power stations. Power stations used seawater to condense steam from turbines. In a typical condenser, seawater temperature is increased by 10-20 °C. To make use of this energy, a low temperature vacuum desalting installation and heat pumps were introduced. The heat pump used is of the absorption type, where it consumes less electrical energy. Further studies showed that the specific thermal energy consumption at desalination plants with absorption heat pumps is 2-2.5 times lower than other power systems.

Reali [1984] proposed a desalination method called the refrigerator-heat pump desalination scheme (RHPDS). In this study, sea water was evaporated and condensed using a vapor compression heat pump. The system consists of two tanks, to contain salt and fresh water, connected at the top part. The tanks were evacuated, and seawater entered the salt water tank at atmospheric pressure. The heat pump will provide heating to evaporate seawater, and cooling to condense the vapors into the fresh water tank. The system was designed to operate with small temperature difference, around 5 °C, for the water tanks. Thus a high energy efficiency was expected.

To utilize solar energy in desalination processes, solar stills are commonly used to evaporate salt water in a basin. Many studies have been conducted on solar still desalination, and many attempts have been made to increase its efficiency. Rahim [2001] conducted a study to increase the solar still's performance. His attempt included applying

forced condensation method in the solar still. With this method vapors were sucked from the still's evaporator zone and condensed over copper tubes that run in the salt water basin, thus not allowing the vapor to condense on the glass cover's surface. With this method, the unit efficiency increased from 19.41% to 29.55%. Rahim [2003] also proposed the idea to store excess heat absorbed by solar stills by separating the basin into evaporating and heat storing zones. The division of the basin is achieved by placing an aluminum plate slightly below the water surface, with gaps between the plate's edges and the basin wall, thus still allowing water to form a thin layer on the plate surface. This technique, which does not require any external power to store heat, enables the unit to recover 47.2% of the energy absorbed in the day during night operation. The unit has an average efficiency of 57.3%, which is 12.5% higher than the average efficiency of similar size basin unit.

Sinha and Tiwari [1992] conducted an analysis of a concentrator assisted solar distillation unit. The unit consist of a solar still coupled to a non-tracking cylindrical parabolic concentrator. The water in the basin is circulated into the concentrator by an electric pump, thus the salt water receives more heat from the circulation. The unit produced a maximum yield of more than 8 l / m² day for a water depth of 0.02 m. At 0.1 m deep the unit yields around 6 l / m². The overall thermal efficiency of the unit at each depth is around 45 and 30%, respectively. A different type of solar still used for desalination was studied by Minasian and Al-Karaghoulis [1992]. They studied the performance of a conical still floating in a salt water basin. The conical still consists of a cone-shaped glass cover with a cotton wick formed into the same shape placed inside the cone. The base of the cone enables the wick to absorb water from the basin, thus through capillarity ascension,

water will be absorbed by the conical wick, and solar radiation is absorbed from the cover. The solar still has an average value of distillate output between the range of 2 and 4 liters / m² per day.

Bohner [1989] presents an idea of a 100% solar powered desalination plant. The plant has a water production capacity of 2 to 20 m³ / day. The product water can be used as a potable water or for agricultural applications. The plant is operating in a low temperature range of 65 to 75 °C. A small amount of electrical demand is used for circulation pumps, which can be produced from a photovoltaic system or from a wind turbine. The first pilot plant was built in Laatzen/Hannover in 1988 to conduct initial experiments.

Le Goff et al. [1991] developed a design of a multi stage solar still. The unit consisted of a stack of six rectangular vertical walls. Salt water flows in between each wall. Heated by solar radiation, the salt water evaporates and condenses on the opposite wall. The heat from the condensed vapor is used to evaporate salt water on the other side of the wall. The unit is capable of producing more than 20 litres of distilled water per m². The advantage of the design is that it is simple, rugged, easy to maintain by any craftsman with technical skills, thus making it ideal to be used in remote rural areas.

Hawlder et al. [2004] conducted a study on a solar assisted heat pump desalination system. The system consists of a solar assisted heat pump, a distillation chamber, and a solar water preheating unit. The heat pump used an unglazed, serpentine tube solar evaporator collector. Feed water is preheated through a commercial solar liquid collector, and upon entering the evacuated distillation chamber, undergoes thermodynamic flashing.

The heat pump then provides further evaporation of remaining water and condensation of vapors in the upper section of the chamber. Performance analysis showed that the performance ratio of the system ranges from 0.77 to 1.15, while the coefficient of performance ranges from 5.0 to 7.0.

Kudish et al. [2003] developed and tested a solar desalination system using an evaporator / condenser chamber. The system is constructed fully of polymeric materials to prevent corrosion from salt water. A simulation model was developed and validated with experimental measurements of the system's performance. The model was then used in a parametric study to determine optimum design. Based on the prototype system, it was found out that the system is capable of producing 11 kg / m² per day of fresh water on a sunny day with the gap between evaporator and condenser surfaces is close to 2 cm, and the feed flow rate is within the range of 40 – 50 kg / m² day.

A small solar water desalination unit was constructed and investigated by Nafey et al. [2007]. The system uses the solar flat plate collector as a brine heater, and is attached to a vertical flashing/condenser unit. The heated water from solar collector is flashed in the unit, latent heat of vaporization is used to preheat feed water and condense the vapor. The average productivity of the system in November to January ranged between 1.04 to 1.45 kg/ m² day. The average summer productivity ranged between 5.44 and 7 kg/ m² day in July and August, and 4.2 and 5 kg/ m² day in June. The unit has a performance ratio of 0.7 to 0.8 in winter, and 0.8 to 0.9 in summer.

Al-Kharabsheh and Goswami [2004] proposed an innovative concept of water desalination using low grade solar heat. The system uses natural forces of gravity and atmospheric pressures to create vacuum in an evaporation chamber, which enables continuous flow of water from a source tank thus removing the necessity of a pump. Saline water in the vacuum chamber will then be evaporated by solar energy. Evaporated water is then condensed into another tank. Through numerical simulations, the system showed that it has an efficiency as high as 90%.

El-Nashar [2000b] developed a simulation program to predict the performance of a solar desalination plant. The plant consisted of evacuated tube solar collectors, a heat accumulator tank, with water as the working fluid, and MED chambers. The absorber area of the collector field varied between 500 and 20000 m², with the heat accumulator storage capacity per collector area varies between 0.05 and 1.00 m³/m². Simulation results were validated with a measured data from a solar plant of similar design located in Abu Dhabi, United Arab Emirates. The plant has been in operation since 1984, and meteorological data of the plant collected in 1985 were used in the simulation program. The simulation results showed a good agreement with the measured data for the months of January and June.

Hermann et al. [2002] conducted a study on the desalination of seawater inside solar collectors. The pilot plant, located in Pozo Izquierdo, Gran Canaria, produced about 600 l of drinking water per day. The plant operates at ambient pressure, with temperature range of 70 to 120 °C. The concept of the system is to increase efficiency by allowing seawater to flow directly inside flat plate collectors, thus a corrosion free collectors and materials

are needed. A prototype of the collector has been developed, it consist of a selectively coated glass tubes mounted in a conventional flat-plate collector casing.

A large scale solar desalination scheme was proposed by Rajvanshi [1980]. The scheme was meant to be applied in the Thar Desert region of India to supply the locals with potable water. The method was to pump seawater from the Gulf of Kutch to the southwestern region of the desert. There the sea water was heated in a solar field, and desalinated with a multi stage-flash system. The solar field consisted of a series of rectangular collector tubes, made of concrete, half buried in the ground. In the proposed scheme, there are two series of solar field, each with an area of 9.6 km x 0.6 km, half-buried in the ground 8.9 cm deep. The purpose of the study was to look at the technical and economical feasibility of the system to be applied in the Thar Desert in India. Based on the study, it was concluded that, at a feed flow rate around 2.16×10^5 m³/hour, the system will be able to produce 5.25×10^7 m³ of fresh water per year. An area of 11.52 km² will be needed to achieve this objective. The pumping requirements for the whole scheme will be supplied by 415 wind turbines, each operating at a 200 kW capacity. The cost of water for the scheme would match that of a fuel-fired MSF plant within 8 years.

Rodriguez et al. [2002] studied the usage of solar energy for desalination processes under Spanish climatic conditions. They compared the use of static and one-axis tracking collector technologies. The case study conducted here is related the use of solar energy in Multi Effect Distillation (MED) and Multi Stage Flash (MSF) systems. The heat input is considered to be at around 65-75 °C for MED and 80-90 °C for the MSF plant. Various solar collector systems were considered, such as Solar Ponds, Flat Plate Collectors, and

Direct Steam Generation (DSG) Parabolic Troughs. At Spanish climatic conditions, DSG-Parabolic Trough showed interesting potential when combined with conventional energy systems. Another advantage of one-axis tracking collectors was that it could be coupled to a heat pump in a desalination plant.

2.3. Economic Analysis of Solar Energy Processes

El-Nashar [2000a] conducted a study on the economics of solar assisted multiple stack distillation plants. Three system configurations were taken into account. The first one is a Multiple Effect Stack (MES) evaporator supplied by steam from a low pressure boiler, and pumping power supplied by a diesel generator. The second mode of configuration used solar thermal collectors to provide thermal energy in the form of hot water to the MES evaporator with pumping power delivered by diesel generator. The third configuration considered a stand-alone system, using 100% solar energy. Thermal energy will be provided by solar collectors, while electricity for pumping power comes from photovoltaic cells. Two cost parameters were taken into account: collector cost per square meter and the cost of diesel oil per giga Joule. The water price from the second configuration was found to be more competitive when compared with the first one if collector cost drops to \$200/m² and diesel oil cost to \$50/GJ. With 100% solar powered, the economics tend to improve in favor to the solar system. Even when diesel oil price reached \$10/GJ, the water price from the solar system approached that of a conventional plant if collector costs \$200/m². The cost of water from the solar system was shown to be always higher than conventional plant when oil price is \$10/GJ, but lower than conventional plant if the fuel price reaches \$50/GJ.

Wijeysundera and Ho [1985] investigated four different economic indices to find optimal sizing of thermal insulation, recovery heat exchangers, and solar heating systems. The economic indices used are annualized cost, life cycle savings, internal rate of return, and payback period. The results gave two optimum sizes, which correspond to maximum life cycle savings and minimum payback period. Further analysis of the optimum sizes for solar heating systems showed that the size that maximizes the life cycle savings was always larger than the internal rate of return. Similar method of economic analysis was conducted by Hawlader et al. [1987] to a solar water heating system in the Changi International Airport in Singapore. The system was designed to provide hot water for the kitchen in the airport. It was found, using life cycle savings and annual life cycle cost calculations, that the optimum collector area was around 1200 m², while analyses using the payback period and internal rate of return indicated an optimum collector area of 1000 m². For the economic variables used in these analyses, the minimum payback period is around 14 years, which was considered rather high.

From the reviewed literature, the following is a summary of important findings:

- The most popular thermal desalination method today is the Multi Stage Flash, with Multi Effect Distillation showing great potential for future development.
- Of the membrane processes the Reverse Osmosis method is still dominant, covering a fairly large share in the market.
- Heat pump systems showed interesting possibilities to be used in desalination systems. Absorption and vapor compression systems have been studied, and few studied the use solar assisted-heat pump in desalination system.

- Solar thermal energy is mainly used in the form of solar stills to desalinate water. There have been many attempts to improve the performance of the solar still.
- Economic analyses showed that with the rising of oil fuel cost, solar thermal energy becomes a promising source of thermal energy.

Based on the above, not many studies have been done on the scope of solar assisted-heat pump desalination systems. Further study is needed in this field to determine the full potential of solar energy and heat pump desalination. Therefore, an experimental setup has been constructed to achieve this goal. Experiments were conducted followed by a simulation study. An economic optimization based on the analytical method mentioned above may be used to determine the feasibility of the system.

Chapter 3

EXPERIMENTS

To facilitate the study, a solar assisted heat pump desalination (SAHPD) system was constructed, and experiments were conducted to evaluate its performance. The system is located on the rooftop of block EA of the National University of Singapore. This chapter describes the main components of the system and its working principles.

3.1. Working Principle of the SAHPD

The system consists of two main parts, a solar assisted heat pump, with refrigerant as its working fluid, and a water desalination section, which preheats and distillates water, as shown in Figure 3.1.

The solar assisted heat pump provides heating and cooling to the desalination process, with a serpentine tube solar evaporator collector that absorbs solar radiation and ambient energy. Refrigerant R134a is used as the heat pump's working fluid. The serpentine tube, with 9.52 mm diameter was soldered at the back of the absorber plate. The bottom of the collector was insulated with polyurethane material. An open type reciprocating compressor, directly coupled to a three phase induction motor was used in the system. A frequency inverter controls the speed of the motor. Refrigerant passes through condenser coil, located at the bottom of the desalination chamber. To ensure complete condensation of the refrigerant, it is allowed to pass through a 250 l water tank. A thermostatic expansion valve regulates the refrigerant's mass flow rate. After passing through the expansion valve, the refrigerant is divided into two branches, one through the evaporator-

collector, and the other to a cooling coil located at the top of the desalination chamber to condense water vapors. These two streams are then mixed before entering the compressor. In the desalination section, a commercial solar collector is used to preheat incoming feed water. An electrical heater is positioned at the outlet of this solar collector to provide auxiliary heating to ensure the feed water to maintain the desired temperature, when solar radiation is inadequate. The electrical heater will maintain the water temperature to be not less than 70°C . After passing through the electrical heater, feed water enters the desalination chamber. The chamber is evacuated to a pressure of 0.14 bar and at this pressure the corresponding saturation temperature for water is 52.6°C . Thus, feed water entering the chamber will undergo thermodynamic flashing. The remaining part of water that does not evaporate will flow down to the bottom of the chamber, where it will be heated further by the heat pump's condenser coil, thus evaporating the water. Vapor from flashing and evaporation will be condensed at the top section of the chamber by a cooling coil of the heat pump. Distillate water produced will flow down to a collection tray.

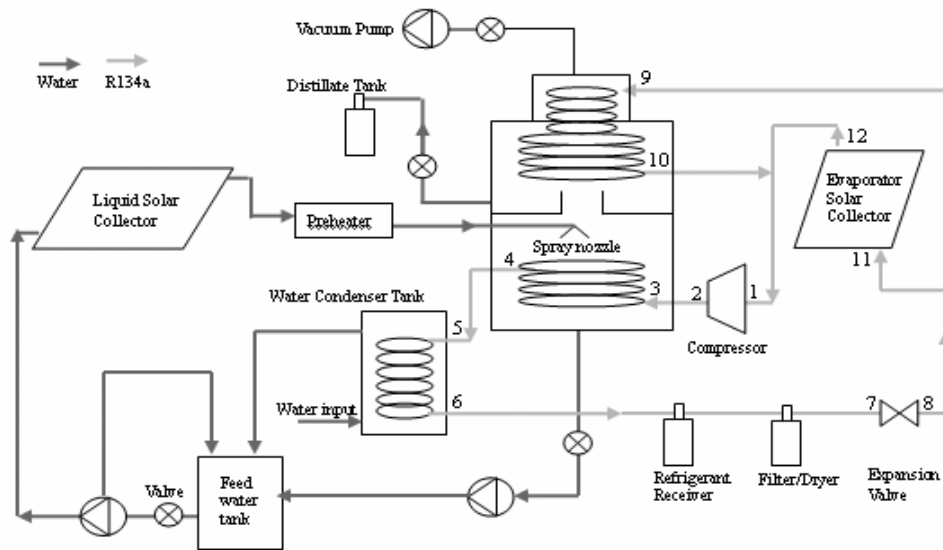


Figure 3.1. Solar assisted heat pump desalination system setup

3.2. Components of the system

The following sections describe the main components of the SAHPD system.

3.2.1. Evaporator collector

The solar collector used in the heat pump system is of the plate and serpentine-tube type, as shown in Figure 3.2(a). Refrigerant entering the collector absorbs heat along the tube, evaporated, and reaches a superheated state at the exit. The evaporator collector is unglazed to allow it to absorb heat from ambient, as the operating temperature is usually less than the ambient. The collector has an area of 1.5 m^2 , with an insulation made of polyurethane 50 mm thick at the bottom part of the collector. The collector has a tube spacing of 100 mm, and the plate is made of 1 mm thick copper.

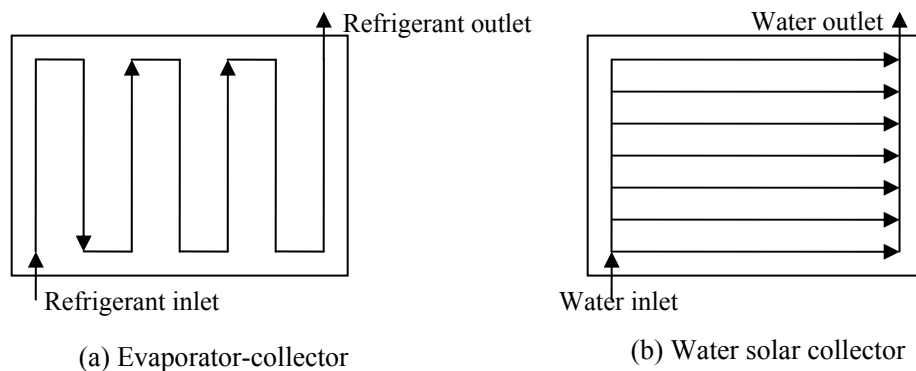


Figure 3.2. Schematic diagram of (a) evaporator-collector and (b) water solar collector

3.2.2. Liquid collector

A commercial solar water collector is used to preheat the feed water, as shown in Figure 3.2(b). It has an area of 2 m^2 and 50 mm thick insulation at the bottom of the collector. The collector is of parallel tube-type, with seven riser tubes connected by two headers.

The plate is made of 0.9 mm thick aluminum. The collector is glazed with 3mm thick glass to reduce heat loss to the environment.

3.2.3. Compressor

The compressor used in the system is of the single cylinder-reciprocating type. It is connected to a three phase induction motor, and the speed of the compressor is controlled with a frequency inverter. The compressor has a capacity of 1.5 kW with a maximum 50 Hz operating frequency. Figures 3.3 and 3.4 show the compressor and frequency inverter.



Figure 3.3. Compressor



Figure 3.4. Frequency inverter

3.2.4. Thermostatic expansion valve

A thermostatic expansion valve, as shown in Figure 3.5, is used in the system to reduce refrigerant pressure after leaving the water condenser tank to evaporator pressure.

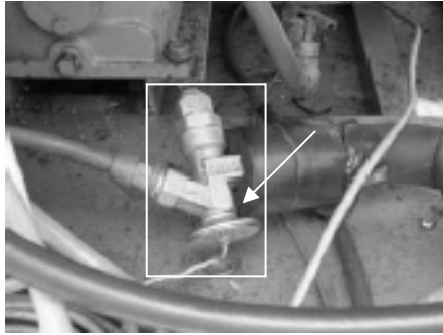


Figure 3.5. Thermostatic expansion valve

3.2.5. Water condenser tank

The condenser tank, as shown in Figure 3.6, has a volume of 250 liter. During the experiments it is filled with water. A 25 m long copper coil with an outer diameter of 9.52 mm is submerged inside it. Water in the tank will absorb heat from the coil, to ensure complete condensation of the refrigerant vapor before it approaches the expansion valve. The condenser tank is insulated with polyurethane and covered with aluminum casing.



Figure 3.6. Water condenser tank

3.2.6. Desalination chamber

The desalination chamber, as shown in Figure 3.7, is made of PVC. It is cylindrical in shape, with a 255 mm diameter and 500 mm height. During the experiment, the chamber is evacuated to a pressure of about 0.14bar. To monitor the pressure inside the chamber, a pressure gauge is mounted at the top of the chamber. At this low pressure, water saturation temperature is at 52 °C. With feed water entering at 70 °C, thermodynamic flashing occurs in the chamber. Feed water enters the chamber through a spray nozzle. This nozzle will generate droplets falling over a condenser coil located at the bottom of the chamber. A tray is located at the upper part of the chamber. An evaporator with a 3.3 m long copper coil is located at the top to condense the vapors generated from flashing and evaporation.



Figure 3.7. Desalination chamber

3.2.7. Electrical heater

An electrical heater is positioned after the liquid solar collector. The heater maintains the feed water to a set temperature before entering into the desalination chamber. It has a rating of 2.24 kW, and contains 6.95 liter of water. During the experiment, the heater is set to maintain feed water temperature at 70°C.

3.2.8. Pumps

There are three different pumps used in the experiment, each with its own distinct function. A single stage belt-driven vacuum pump was used to evacuate the desalination chamber. The vacuum pump has a flow rate of 0.064 m³/minute. This pump is connected to the top of the chamber. The pressure inside the chamber is maintained at 0.14 bar by the vacuum pump.

To remove excess water from the bottom of the chamber, a positive displacement pump was used.

To circulate the feed water from the feed water tank to the chamber, a commercial water pump was used. A bypass connection is applied to the pipeline at the outlet of the pump to control the flow rate of the water.

3.3. Instrumentation

Temperatures of the refrigerant and feed water were measured using T-type thermocouples. Prior to the commencement of the experiments, connections of the thermocouples to the measuring points have been tested to ensure its proper function. Digital pressure transducers were installed in the heat pump section, and analog pressure gauges were mounted on the chamber.

To measure solar radiation, a pyranometer was mounted near the system. The pyranometer has a sensitivity of $8.88 \times 10^{-6} \text{ V/m}^2$.

To record the measurement made during the experiment, a 20 channel data logger was placed in a compartment located below the solar assisted heat pump, protected from solar radiation. The readings were taken at 5 minutes interval. In summary, table 3.1 shows the main components of the SAHPD system.

Table 3.1. Summary of main components

Evaporator collector	
Dimensions	1000x1500x50 mm
Plate material	copper
Tube material	copper
Tube outer diameter / thickness	9.5 mm / 1 mm
Tube length	28.4 m
Tube spacing	100 mm
Insulation	Polyurethane
Insulation thickness	50 mm
Compressor	
Bore	35 mm
Stroke	26 mm
Capacity	1.5 kW
Water condenser tank	
Volume	250 liters
Dimensions	500x500x1000 mm
Insulation	Polyurethane
Insulation thickness	50 mm
Tube outer diameter / thickness	9.5 mm / 1 mm
Tube length	25 m
Liquid solar collector	
Dimensions	1000x1980x80 mm
Tube material	copper
Plate material	aluminum
Tube outer diameter / thickness	12.7 mm / 0.7 mm
# of headers	2
# of risers	7
Tube spacing	130 mm
Insulation material	Insulwool
Distillation chamber	
Volume	25.5 liters
Outer diameter	255 mm

Table 3.1 (Continued)

Height	500 mm
Chamber material	PVC
Coil material	copper
Length of cooling coil	3.5 m
Length of condenser coil	2 m
Tube outer diameter / thickness	9.5 mm / 1 mm

3.4. Test Procedure

Prior to running the system, it is necessary to check the weather conditions. Cloudy days are not desirable to conduct experiments, as the liquid solar collector will not be able to absorb much heat. Other than weather conditions, there is a list of other conditions shown below that needs to be fulfilled before running the system:

1. The water condenser tank must be filled with water, with the coil submerged.
2. The valves of the water line are in their desired positions.
3. There is adequate refrigerant pressure in the solar assisted heat pump.
4. The feed water tank is filled with clean water.
5. The electric heater is set to 70°C.

If such conditions are met, then the experiment may be conducted according to the following procedure:

1. Turn on the main power switch to the system.
2. Turn on the positive displacement pump to drain any remaining water in the chamber.
3. Turn on the vacuum pump to lower the chamber's pressure to 0.14 bar.
4. Put the pyranometer in an open place, make sure it is not obstructed.
5. Put the data logger in place, set it to measure the readings from the sensors.
6. Set the desired frequency of the compressor, and activate it.

7. Open the valve of the feed water tank, run the water circulation pump.
8. Activate the electrical heater.
9. After a few minutes, the system will reach steady state condition. Set the data logger to record the measurements.

To shut down the system, the following procedure is to be followed. These are listed below:

1. Turn off the compressor, vacuum pump, electric heater, and water circulation pump. Let the compressor cool down for about 10 minutes.
2. Open the feed water valve located near the chamber slowly to collect the desalinated water.
3. Let the positive displacement pump run for a little while to drain the remaining water in the chamber. Turn it off after it finishes draining.
4. Stop the data logger from recording and turn it off.
5. Store the pyranometer back to its case.
6. Cover the whole system, turn off the main power switch, take the pyranometer and data logger back to the laboratory.

CHAPTER 4

MODELING, SIMULATION, AND OPTIMIZATION

Mathematical equations describing the performance of different components of the solar assisted heat pump desalination system are described in this chapter. The MATLAB programming language was used in running the simulation program. Equations describing the economic optimization Figures are also presented. The economic Figures of merit taken into consideration are the annual cost, life cycle savings, and payback period.

4.1. Modeling of Components

This section explores the mathematical modeling of the system. The main components covered in the model are the evaporator and liquid solar collector, compressor, expansion valve, condenser tank, and desalination chamber.

4.1.1. Liquid solar collector

The liquid solar collector used to preheat the feed water has a single glazing, with an aluminum plate as the absorber. The collector is of parallel tube-type, with seven riser tubes positioned in parallel with the collector's length. Several assumptions are made to model the collector:

1. The collector is operating in steady-state condition.
2. The headers do not affect the thermal process and efficiency of the collector.
3. There is a uniform flow of water inside the tubes.
4. Heat flow is one dimensional, from the covers to the insulation.
5. Collector properties are independent of temperature.
6. The solar radiation falling on the cover is of uniform value.

The useful energy absorbed by the water, in terms of its inlet and outlet temperature is expressed as:

$$Q_u = \dot{m}_w c_{p,w} (T_{w,out} - T_{w,in}) \quad (4.1)$$

The useful energy delivered from the collector to the water can be expressed through the Hottel-Willier equation [Duffie, 1980]:

$$Q_u = F_R A_C [I(\tau\alpha) - U_L (T_{in} - T_a)] \quad (4.2)$$

In terms of mean plate temperature, the useful energy can also be expressed as:

$$Q_u = A_C [I(\tau\alpha) - U_L (T_p - T_a)] \quad (4.3)$$

where T_p denotes the mean plate temperature.

Overall heat loss coefficient, U_L , of the collector is a function of the top, bottom, and edge losses. Edge losses are usually negligible for a well designed collector [Duffie, 1980], thus, the overall loss becomes:

$$U_L = U_T + U_B \quad (4.4)$$

The top loss coefficient, U_T , can be expressed as:

$$U_T = \left\{ \frac{N}{\frac{C}{T_p} \left[\frac{T_p - T_a}{(N + f)} \right]^e} + \frac{1}{h_w} \right\}^{-1} + \frac{\sigma(T_p + T_a)(T_p^2 + T_a^2)}{(\varepsilon_p + 0.00591Nh_w)^{-1} + \frac{2N + f - 1 + 0.133\varepsilon_p - N}{\varepsilon_g}} \quad (4.5)$$

Where N is the number of glass covers. Several other correlations were simplified to fit the equation (4.5). These are:

$$f = (1 + 0.089h_w - 0.1166h_w\varepsilon_p)(1 + 0.07866N) \quad (4.6)$$

$$e = 0.43(1 - 100/T_p) \quad (4.7)$$

$$C = 520(1 - 0.000051\beta^2) \quad (4.8)$$

For $0^\circ < \beta < 70^\circ$. For $70^\circ < \beta < 90^\circ$, use $\beta = 70^\circ$

The bottom loss coefficient, U_B , is defined as:

$$U_B = \frac{k}{t} \quad (4.9)$$

With k is the thermal conductivity of the insulation material, and t is the insulation's thickness.

The collector heat removal factor, F_R , is a quantity that relates actual useful energy gain of a collector to the useful gain if the collector surface is at liquid inlet temperature. This value can be expressed as [Duffie, 1980]:

$$F_R = \frac{\dot{m}c_p}{A_c U_L} (1 - e^{-(A_c U_L F' / \dot{m}c_p)}) \quad (4.10)$$

With F' is the collector efficiency factor:

$$F' = \frac{1}{U_L} \frac{1}{W \left[\frac{1}{U_L [D_o + (W - D_o)F]} + \frac{1}{C_b} + \frac{1}{\pi D_i h_{f,i}} \right]} \quad (4.11)$$

Where D_o is the tube outer diameter, and W is the distance between the center of two tubes, as shown in Figure 4.1.

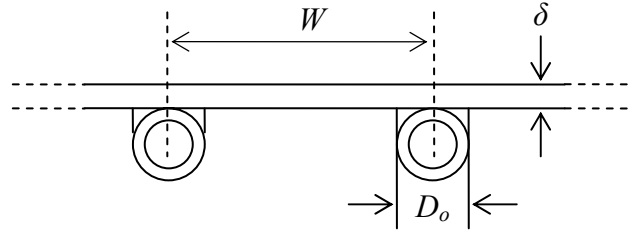


Figure 4.1. Cross section of solar collector

The fluid heat transfer coefficient, for single phase condition, is determined from Dittus-Boelter equation:

$$h_{f,i} = 0.83 \text{Re}^{0.8} \text{Pr}^{0.33} \frac{k_f}{D_i} \quad (4.12)$$

And C_b is the bond conductivity:

$$C_b = \frac{k_b b}{\gamma} \quad (4.13)$$

With k_b is the bond thermal conductivity, b is the bond's width, and γ is the bond average thickness.

The function F in equation 4.11 is the standard fin efficiency. It is described as:

$$F = \frac{\tanh[m(W - D_o)/2]}{m(W - D_o)/2} \quad (4.14)$$

Where $m = \sqrt{U_L / k\delta}$

4.1.2. Evaporator Collector

The evaporator collector is an unglazed, serpentine tube-type collector. Refrigerant leaves the collector in a superheated condition. Energy absorbed by the collector can be expressed by equation (4.15), in terms of enthalpy change:

$$Q_u = \dot{m}_{ref, coll} (h_{out} - h_{in}) \quad (4.15)$$

In modeling, the tube of the collector is divided into segments. Each segment received an increase of energy from solar radiation and the ambient. Useful energy absorbed by the evaporator collector is modeled in a similar way to liquid solar collector. The modeling difference of the two collectors lies in the two-phase and superheated regions of the evaporator collector. Within the two-phase region, a different expression to calculate refrigerant heat transfer coefficient was used.

For the evaporator-collector, while the refrigerant is passing through the tubes absorbing ambient and solar energy, it may exist in either two-phase or superheated condition. In the first condition refrigerant is assumed to be in the two-phase region, thus any energy absorbed will be used to evaporate the refrigerant, thus causing an increase of vapor quality, a ratio of mass flow rate of vapor to total mass flow rate of the refrigerant. After the vapor quality reaches $x = 1$, the refrigerant model uses superheat conditions. From this point all energy absorbed will be used to increase the refrigerant's temperature.

To calculate the heat transfer coefficient of the refrigerant in the two-phase condition, Chaturvedi et al., (1982) developed the following correlation.

$$h_{fi} = \frac{0.0082k_f}{D_i} \left\{ \frac{(R_e^2 J \Delta x) h_{fg}}{L} \right\}^{0.4} \quad (4.16)$$

Where J is a dimensional constant with a value of 778, and Δx shows the change of vapor quality within a segment of the tube.

The h_{fi} of equation (4.16) is then used the same way as in equation (4.11) for the two-phase condition of evaporator collector.

Vapor fraction, x , is commonly expressed in the form:

$$h_e = h_{f,sat}(1-x) + xh_{g,sat} \quad (4.17)$$

Rearranging, we get:

$$x = \frac{h_e - h_{f,sat}}{h_{fg}} \quad (4.18)$$

with h_e is the enthalpy of refrigerant in two-phase condition at a certain point in the evaporator collector, $h_{f,sat}$ is the saturated liquid enthalpy of the refrigerant, and h_{fg} is the enthalpy of vaporization of the refrigerant.

4.1.2.1. Pressure drop in evaporator collector

To describe two-phase flows in the collector tube, it is assumed that the two phases are in thermodynamic equilibrium. The change in vapor quality is mainly due to solar and ambient energy input, and quality change due to pressure change can be neglected. For a well-designed collector, the pressure drop through the tube is usually small, and the above assumption is justified [Chaturvedi et al., 1982].

Chaturvedi et al., (1982) developed an equation to model two-phase flow pressure drop in horizontal solar collector tubes. The final form of the equation is described as:

$$\frac{-dp}{dz} = \frac{\frac{2fG^2}{D_i}(v_f + xv_{fg}) + G^2v_{fg} \frac{dx}{dz}}{\left(1 + G^2\left(x\frac{dv_g}{dp} + (1-x)\frac{dv_f}{dp}\right)\right)} \quad (4.19)$$

Where f denotes tube friction coefficient, x is vapor quality, v_f and v_g are specific volumes of saturated liquid and vapor phases and are function of pressure only, and G is the mass flow rate per unit tube area.

4.1.3. Desalination chamber

The desalination chamber used in the experiment provides thermodynamic flashing, evaporation, and condensation processes to take place inside it. Feed water enters the chamber through a spray nozzle to enable uniform flashing. Condenser coil, located at the bottom of the chamber, will provide heat to evaporate feed water that does not evaporate from flashing. Due to buoyancy effect, vapors generated from flashing and evaporation will flow to the top of the chamber, where it will be condensed by the cooling coil, as shown in Figure 4.2.

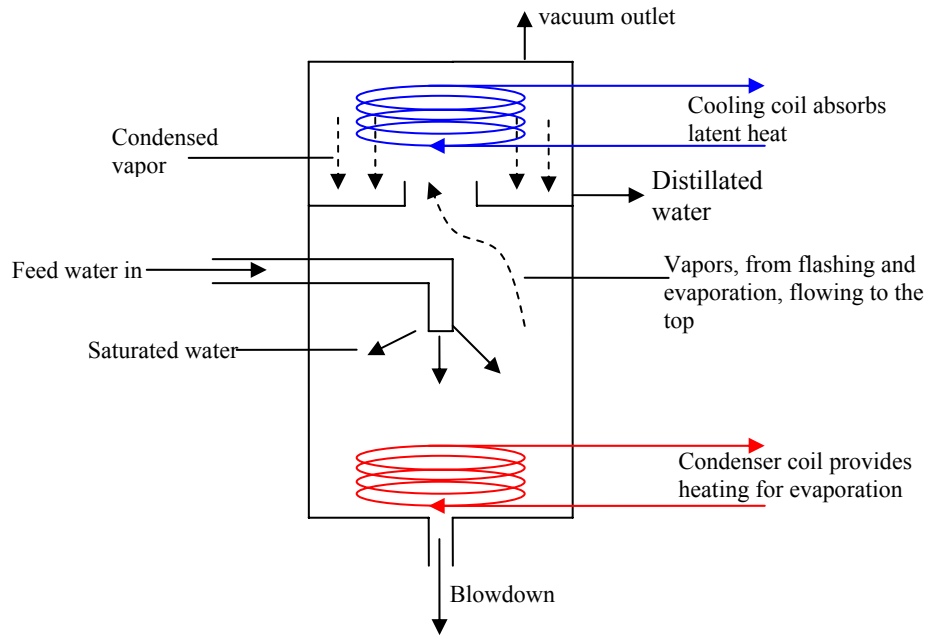


Figure 4.2. Heat transfer processes taking place inside the desalination chamber

To model the chamber, it is assumed to have similar characteristics of a one pass, single tube heat exchanger at the condenser and cooling coil section. Thermodynamic flashing is assumed to occur at equilibrium condition.

Therefore, mass of vapor produced due to flashing can be expressed as:

$$\dot{m}_v = \frac{\dot{m}_{feed} c_{p,wtr} (T_{feed} - T_{chamber})}{h_{fg,wtr}} \quad (4.20)$$

Thermodynamic flashing occurs at 52°C, which corresponds to chamber inner pressure of 0.14 bar.

Thermodynamic flashing produces saturated vapor and liquid water. Saturated liquid water will then be evaporated by the heat released from the condenser coil. The condenser coil behaves like that of a heat exchanger, therefore, the amount of heat released by the condenser coil can be described as:

$$Q_{condenser} = \varepsilon C_{\min} (T_{h,i} - T_{c,i}) \quad (4.21)$$

Where $T_{h,i}$, inlet temperature of hot fluid refers to refrigerant inlet temperature, and $T_{c,i}$, inlet temperature of cold fluid refers to saturated liquid water. In the equation, the *effectiveness-NTU* method is used. Effectiveness, ε , is the ratio of actual heat transfer rate of a heat exchanger to maximum possible heat transfer rate.

$$\varepsilon = \frac{Q}{Q_{\max}} \quad (4.22)$$

C_{\min} is a product of fluid mass flow times its heat capacity. Since there are two fluids, hot and cold, C_{\min} is the value of the smaller product. In other words:

$$\begin{aligned} C_C &= \dot{m}_c c_{p,c} \\ C_H &= \dot{m}_H c_{p,H} \end{aligned} \quad (4.23)$$

If $C_C < C_H$, then $C_{\min} = C_C$ and $C_{\max} = C_H$. Consequently, if $C_H < C_C$, then $C_{\min} = C_H$ and $C_{\max} = C_C$. In heat exchanger equations, it is also useful to describe:

$$C = \frac{C_{\min}}{C_{\max}} \quad (4.24)$$

For any heat exchanger, it can be shown that [Incropera et al., 1985]:

$$\varepsilon = f(NTU, C) \quad (4.25)$$

where NTU, number of transfer units, is a dimensionless parameter used in heat exchanger analysis. It is defined as:

$$NTU = \frac{UA}{C_{\min}} \quad (4.26)$$

where A is the area of heat exchange surface, and U is the overall heat transfer coefficient.

Overall heat transfer coefficient is defined as:

$$U = \frac{1}{\frac{1}{h_o} + \frac{r_o}{k} \ln\left(\frac{r_o}{r_i}\right) + \frac{1}{h_i} \left(\frac{r_o}{r_i}\right)} \quad (4.27)$$

In the equation (4.27), h_o and h_i are the heat transfer coefficients of fluids outside and inside of the tube, respectively, as shown in Figure 4.3.

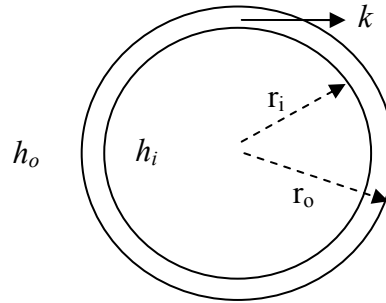


Figure 4.3. Cross section of heat exchanger tube

For a one pass-single tube heat exchanger, the effectiveness is defined as [Becker, 1986]:

$$\varepsilon = 2 \left[1 + C + \sqrt{1 + C^2} \frac{1 + \exp\left(-NTU \sqrt{1 + C^2}\right)}{1 - \exp\left(-NTU \sqrt{1 + C^2}\right)} \right]^{-1} \quad (4.28)$$

Condensation occurs in the top section of the chamber due to the cooling coil absorbing latent heat from the vapor. The cooling coil functions as a heat exchanger to condense the

vapors. In heat exchanger analyses, for condensation taking place outside a horizontal tube, the average heat transfer coefficient is described in the form [Incropera, 1985]:

$$\bar{h}_D = 0.728 \left[\frac{g \rho_l (\rho_l - \rho_v k_l^3 h_{fg})}{\mu_l (T_{sat} - T_s) D_o} \right]^{1/4} \quad (4.29)$$

Thus, the amount of heat absorbed and released by the refrigerant, in cooling coil's condensation and condenser coil's evaporation processes, respectively, will be proportional to the amount of water condensed / refrigerant evaporated.

$$\dot{m}_{condensed,water} = \frac{Q_{cooling,coil}}{h_{fg,water}} \quad (4.30)$$

$$\dot{m}_{evaporate,refrigerant} = \frac{Q_{condenser}}{h_{fg,refrigerant}} \quad (4.31)$$

4.1.4. Compressor model

A reciprocating compressor coupled to an electric motor and a frequency inverter is used in the system. The frequency inverter is used to control the running speed of the compressor. The compressor model is assumed to have a polytropic index of n .

Volumetric efficiency of the compressor can be expressed as [Brown, 2005]:

$$\eta_v = 1 + C - C \left(\frac{p_2}{p_1} \right)^{1/n} \quad (4.32)$$

Mass flow rate flowing through the compressor can be expressed as:

$$\dot{m} = \frac{V_d N \eta_v}{v_1 \times 60} \quad (4.33)$$

Work required to run the compressor:

$$W_C = \dot{m} \frac{p_1 v_1}{\eta_v} \frac{n}{n-1} \left[\left(\frac{p_2}{p_1} \right)^{\frac{n-1}{n}} - 1 \right] \quad (4.34)$$

Discharge temperature of the refrigerant:

$$T_{c,o} = T_{c,i} \left(\frac{p_2}{p_1} \right)^{\frac{n-1}{n}} \quad (4.35)$$

4.1.5. Condenser model

The water condenser tank is used to cool down the refrigerant leaving the condenser coil of the distillation chamber. The condenser consists of a tube coil immersed in water in a tank. Refrigerant flowing inside the tube will release its heat to the water. In the model, the water temperature in the tank is assumed to be uniform, hence a mixed tank model is used for this analysis.

Heat rejected in terms of maximum temperature can be expressed as:

$$Q_{cond} = \dot{m}_w c_{p,w} \varepsilon_{cond} (T_{h,i} - T_{c,i}) \quad (4.36)$$

Heat rejected by the refrigerant can be expressed as:

$$Q_{r,cond} = \dot{m}_r (h_{r,in} - h_{r,out}) \quad (4.37)$$

And the heat absorbed by the water as:

$$Q_{w,cond} = \dot{m}_w c_{p,w} (T_{w,out} - T_{w,in}) \quad (4.38)$$

4.1.6. Thermostatic expansion valve

The expansion valve is located in the refrigerant path after leaving the condenser. Its main function is to reduce the pressure of the refrigerant prior to entering the evaporator collector. The expansion process is assumed to be isenthalpic, therefore:

$$h_{r,i} = h_{r,o} \quad (4.39)$$

4.1.7. Electric heater

The electric heater, located between liquid solar collector and desalination chamber, functions as a booster to preheat the feed water. Therefore, it covers the necessary heat should there be not enough solar radiation. For the experiment, the heater is set to keep the feed water outlet temperature at no less than 70 °C. The energy absorbed by the heater is defined in the form:

$$Q_{electrical} = \dot{m}_{feed} c_{p,water} (T_{out} - T_{in}) \quad (4.40)$$

4.1.8. Performance parameters

For any solar thermal system involving solar collectors, the efficiency of solar collectors will always be needed to observe its performance. Instantaneous efficiency of the collectors is defined as the ratio of useful energy absorbed by the working fluid to the amount of solar radiation falling on the collector.

$$\eta_{collector} = \frac{Q_u}{IA} \quad (4.41)$$

The Coefficient of Performance (COP) is used to describe the performance of a heat pump system. It is defined as the ratio of energy released in the condenser coil and water tank to energy used to run the compressor.

$$COP = \frac{Q_{condenser} + Q_{tank}}{W_{compressor}} \quad (4.42)$$

As for a desalination system, a Performance Ratio (PR) shows how well a system produced water compared to the energy input provided.

$$PR = \frac{2326m_{produced}}{Q_{in}} \quad (4.43)$$

Where 2326 kJ is the theoretical amount of energy needed to evaporate 1 kg of water, and Q_{in} is the electrical energy input to produce $m_{produced}$.

In order to find the solar contribution, a quantity called Solar Fraction is introduced, which is a measure of the solar energy input to total load demand:

$$SF = \frac{Q_{solar}}{Q_{solar} + Q_{electrical}} \quad (4.44)$$

4.2. Meteorological Data of Singapore

Meteorological data is very important in solar thermal systems. They provide the necessary data to perform load calculations. In the solar assisted heat pump desalination system, local meteorological data has been used and will be described in this section.

4.2.1. Singapore's Climatic Conditions

As a country located near the equator (1°21'N, 103°55'E), Singapore has a uniform temperature, high humidity and a reasonable rainfall throughout the year. The daily ambient temperature variation is relatively small, while annual temperature variation is about 1.9°C. The relative humidity is generally high. In the early hours of the morning it reaches around 90%, and drops to around 60% in the afternoon.

There are hardly any seasonal effects. Two main seasons are the Northeast monsoon and Southwest monsoon. Northeast monsoon starts in late November and ends in March, whereas Southwest monsoon usually starts in the second half of May and ends in September. In between these two seasons, there are shorter inter monsoon periods. Rain frequently occurs during the early part of Northeast monsoon.

4.2.2. Correlation for Singapore's Meteorological Conditions

A model to describe Singapore's meteorological condition has been developed by Hawlader et al. (1990). This model predicts the average daily values of solar radiation, ambient temperature, wind speed, and relative humidity of a certain month.

$$X = \sum_{n=0}^7 a_n t^n \quad (4.45)$$

Where X = hourly values of the variables (solar radiation, ambient temperature, relative humidity, and wind speed), a_n = coefficient of polynomial equation, t = station time, which is 7 hours ahead of GMT. The values of the coefficient, a_n , in equation (4.45) are given in Tables 4.1, 4.2, and 4.3.

Table 4.1. Solar radiation coefficients

	January	February	March	April	May	June
a0	1.39E+01	26.299	33.092	2.14E+01	7.55E+00	7.73E+00
a1	-7.0314	-12.174	-15.784	-1.05E+01	-4.26E+00	-4.15E+00
a2	1.1914	2.0026	2.7158	1.82E+00	7.45E-01	6.99E-01
a3	-0.08239	-1.44E-01	-2.09E-01	-1.36E-01	-4.89E-02	-4.36E-02
a4	2.37E-03	4.60E-03	7.37E-03	4.55E-03	1.15E-03	9.13E-04
a5	-2.17E-05	-5.34E-05	-9.76E-05	-5.53E-05	-4.16E-06	-2.94E-07
a6	0	0	0	0	0	0
a7	0	0	0	0	0	0
	July	August	September	October	November	December
a0	3.04E+00	6.58E+00	-4.18E+00	2.11E+01	1.56E+01	1.68E+01
a1	-2.20E+00	-3.82E+00	1.01E+00	-1.03E+01	-8.45E+00	-8.52E+00
a2	3.89E-01	6.74E-01	-1.69E-01	1.77E+00	1.59E+00	1.50E+00
a3	-2.06E-02	-4.46E-02	2.73E-02	-1.33E-01	-1.31E-01	-1.12E-01
a4	1.19E-04	1.10E-03	-1.89E-03	4.48E-03	4.86E-03	3.71E-03
a5	9.64E-06	-5.90E-06	4.24E-05	-5.47E-05	-6.78E-05	-4.39E-05
a6	0	0	0	0	0	0
a7	0	0	0	0	0	0

Table 4.2. Temperature coefficients

	January	February	March	April	May	June
a0	2.20E+01	2.21E+01	2.19E+01	2.28E+01	2.40E+01	2.41E+01
a1	2.93E+00	3.35E+00	4.58E+00	3.95E+00	3.08E+00	2.63E+00
a2	-1.39E+00	-1.59E+00	-2.21E+00	-1.98E+00	-1.60E+00	-1.37E+00
a3	2.53E-01	2.92E-01	4.29E-01	3.96E-01	3.22E-01	2.75E-01
a4	-2.01E-02	-2.37E-02	-3.88E-02	-3.68E-02	-2.99E-02	-2.51E-02
a5	7.31E-04	9.10E-04	1.78E-03	1.74E-03	1.40E-03	1.15E-03
a6	-1.07E-05	-1.51E-05	-3.99E-05	-4.08E-05	-3.24E-05	-2.60E-05
a7	2.66E-08	6.79E-08	3.48E-07	3.77E-07	2.94E-07	2.27E-07
	July	August	September	October	November	December
a0	2.40E+01	2.44E+01	2.34E+01	2.30E+01	2.20E+01	2.21E+01
a1	2.26E+00	1.90E+00	2.93E+00	3.28E+00	3.79E+00	3.06E+00
a2	-1.19E+00	-1.04E+00	-1.52E+00	-1.72E+00	-1.92E+00	-1.47E+00
a3	2.43E-01	2.15E-01	3.09E-01	3.51E-01	3.92E-01	2.81E-01
a4	-2.27E-02	-2.01E-02	-2.09E-02	-3.31E-02	-3.75E-02	-2.44E-02
a5	1.07E-03	9.50E-04	1.39E-03	1.57E-03	1.83E-03	1.04E-03
a6	-2.52E-05	-2.22E-05	-3.31E-05	-3.68E-05	-4.46E-05	-2.07E-05
a7	2.36E-07	2.07E-07	3.14E-07	3.38E-07	4.28E-07	1.49E-07

Table 4.3. Wind speed coefficients

	January	February	March	April	May	June
a0	6.42E-01	3.43E-01	7.62E-01	3.63E-01	1.24E-01	2.54E-01
a1	2.13E+00	1.94E+00	6.40E-01	2.06E-01	7.65E-01	5.56E-01
a2	-1.04E+00	-9.27E-01	-3.53E-01	-2.50E-02	-3.54E-01	-2.03E-01
a3	2.12E-01	1.82E-01	6.73E-02	-1.18E-02	6.38E-02	2.54E-02
a4	-2.08E-02	-1.68E-02	-5.34E-03	3.63E-03	-4.61E-03	-7.21E-06
a5	1.07E-03	8.07E-04	1.98E-04	-3.33E-04	1.26E-04	-1.57E-04
a6	-2.78E-05	-1.92E-05	-3.31E-06	1.25E-05	-1.37E-07	8.51E-06
a7	2.93E-07	1.92E-07	1.89E-08	-1.69E-07	-3.11E-08	-1.35E-07
	July	August	September	October	November	December
a0	3.71E-02	1.11E-01	1.56E-01	-8.62E-02	3.92E-01	8.28E-01
a1	1.34E+00	1.23E+00	8.69E-01	9.79E-01	1.02E+00	1.62E+00
a2	-6.22E-01	-6.11E-01	-3.52E-01	-3.62E-01	-4.85E-01	-8.49E-01
a3	1.15E-01	1.21E-01	5.45E-02	4.88E-02	9.06E-02	1.76E-01
a4	-9.50E-03	-1.08E-02	-2.77E-03	-1.50E-03	-7.55E-04	-1.70E-02
a5	3.71E-04	4.72E-04	-2.11E-05	-1.20E-04	2.99E-04	8.37E-04
a6	-6.34E-06	-9.83E-06	5.18E-07	8.53E-06	-5.25E-06	-2.06E-05
a7	-1.35E-07	7.65E-08	-1.03E-07	-1.45E-07	2.80E-08	2.03E-07

4.3. Simulation Algorithm

To determine the performance of the system, the analytical model of each component was used in a simulation program. Figures 4.4 and 4.5 show the flowcharts of the simulation program and the evaporator collector subroutine. The following is an overview of the simulation's algorithm:

1. Input conditions, such as meteorological conditions, refrigerant temperature leaving the expansion valve, and compressor running frequency, are given.
2. Using the input conditions, the program calculates the temperature at the outlet of the liquid solar collector. The subroutine for the liquid solar collector will also calculate collector efficiency and additional energy input from the electrical heater.
3. Similar calculation methods are used in the evaporator collector subroutine. This subroutine calculates the evaporator collector's efficiency and the refrigerant temperature at the outlet. Initially, based on the refrigerant properties, the

subroutine will determine the phase of the refrigerant, and the corresponding equations used. Useful energy absorbed in each segment of the model will increase the energy level of the refrigerant until its exit condition from the evaporator collector is found. The efficiency of the collector is found from the energy gain of the refrigerant compared to energy absorbed by the collector.

4. Temperature leaving the desalination chamber's cooling coil is assumed. An average value of this temperature and the one at the outlet of the evaporator is calculated. This average value becomes the initial value for the compressor's inlet temperature.
5. The following subroutine calculates compressor work, and the temperature of refrigerant leaving the compressor. The temperature value at the compressor outlet becomes the inlet value for the chamber's condenser coil.
6. The chamber subroutine comes next. It calculates thermodynamic flashing, evaporation, and condensation processes that took place in the chamber. Feed water temperature from the liquid solar collector and heater is used to calculate flashing in the chamber. The remaining amount of water that does not vaporize is assumed to be in saturated liquid state, and it is evaporated by absorbing heat from the condenser coil. Vapor from flashing and evaporation is condensed by the cooling coil. Thus, the chamber subroutine calculates the resulting distilled water, and outlet temperatures of condenser and cooling coils. Temperature at the outlet of cooling coil is compared with the initial assumption, and iteration will be conducted if there is a large difference. Large value difference will have the program iterate the compressor inlet temperature using the new value, thus repeating the calculations.

7. Temperature at the outlet of condenser coil becomes the input for the water condenser tank. This subroutine calculates the temperature leaving the tank.
8. Considering the collector efficiencies, water production, and temperature values at inlet-outlet of condensers and solar collector, the coefficient of performance and performance ratio is calculated.
9. The program displays all the desired values. The results are then saved into MS Excel format.

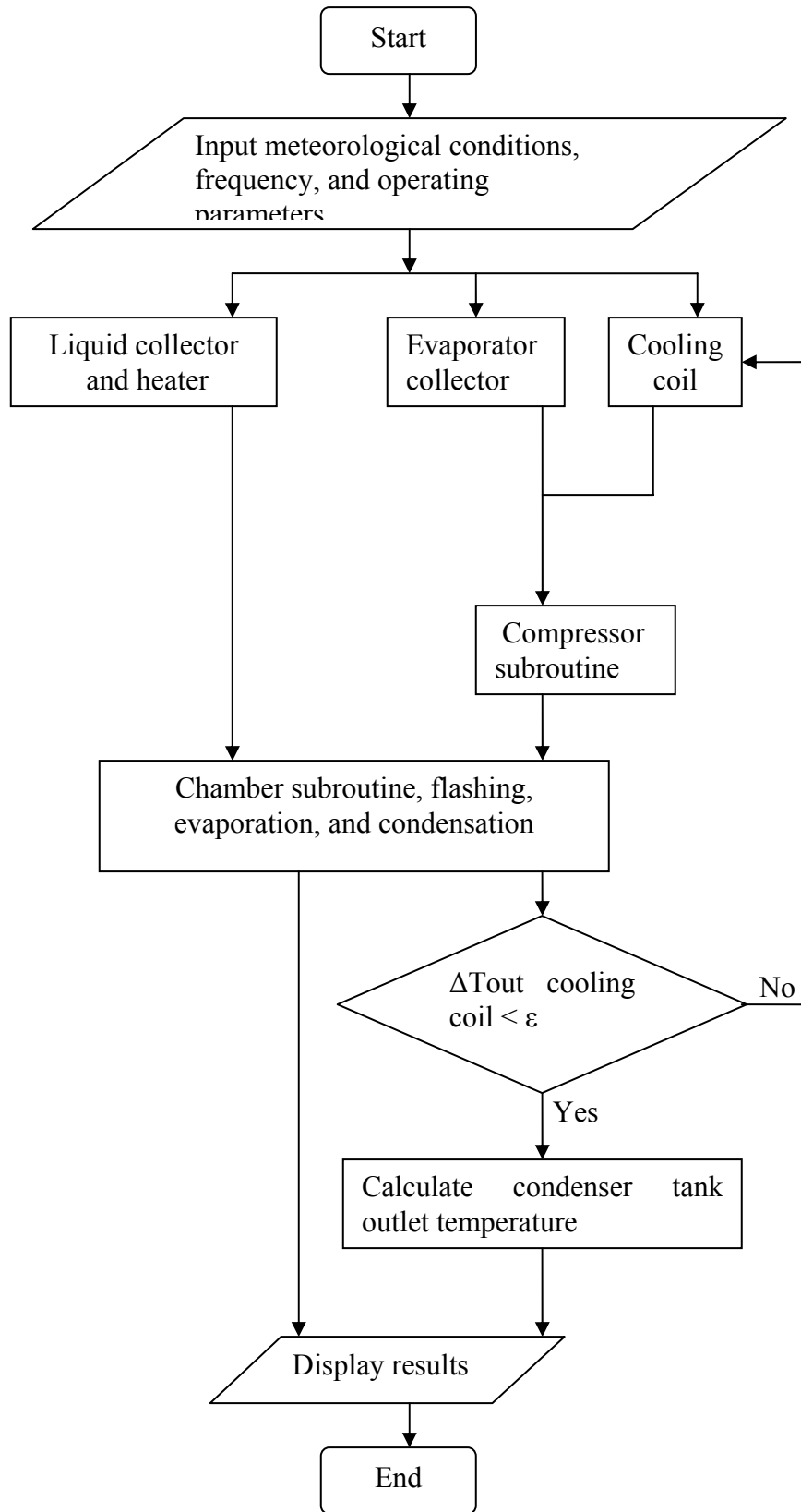


Figure 4.4. Flowchart of the simulation program

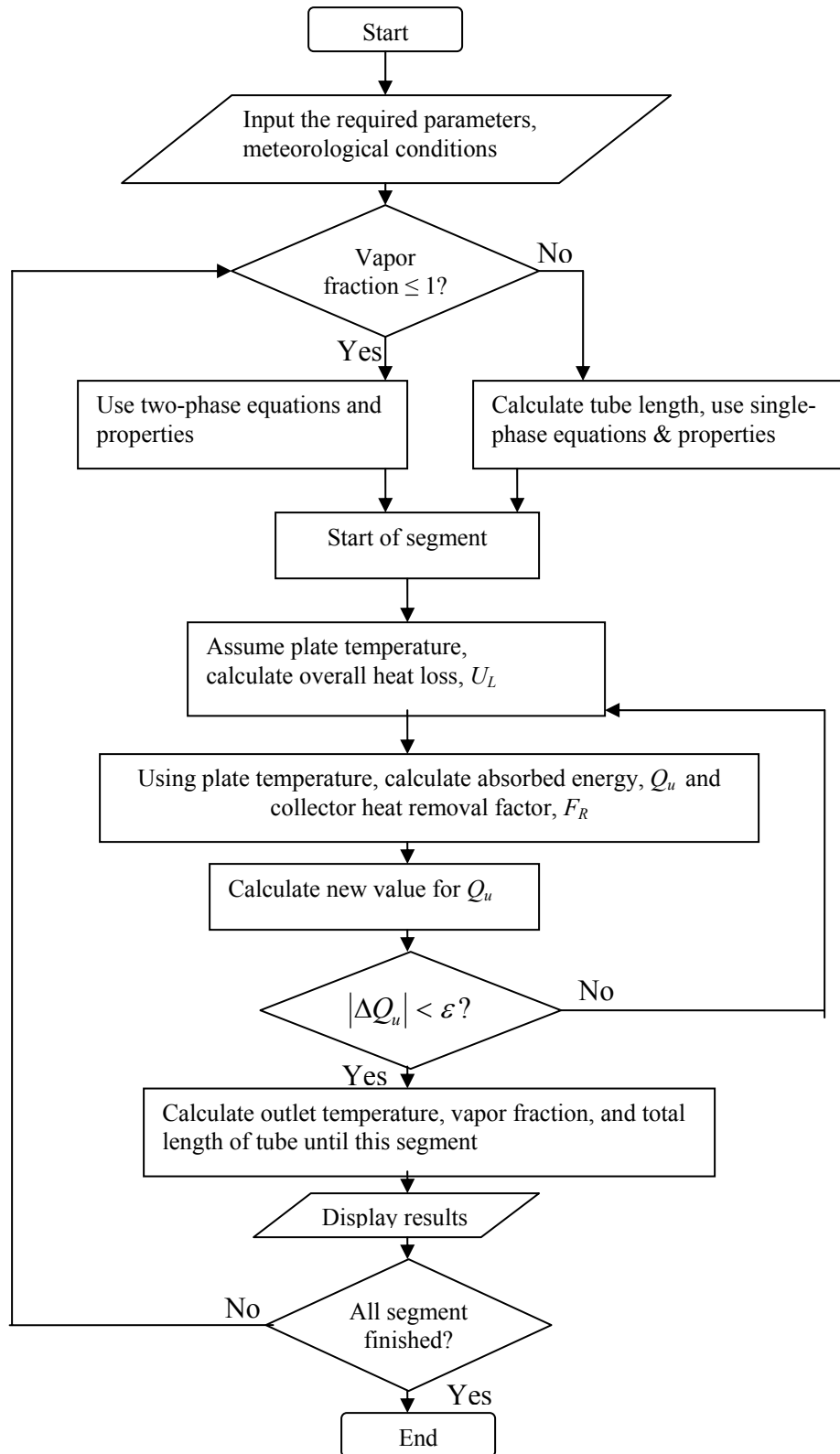


Figure 4.5. Flowchart of evaporator collector

4.4. Economic Optimization

The feasibility of a solar energy system is determined not only from its performance but also from an economic analysis, which must be carried out to evaluate its performance. Usually, solar energy systems require an initial high investment followed by a low maintenance and operation costs [Hawlander et al., 1987]. Therefore, an optimization to determine the system's feasibility must take into account several economic parameters as well.

In general, all components of a solar energy system will affect its performance and also its cost. However, in practice, the problem is often reduced to observe the most influential parameter of the system. As in all solar energy systems, the collector's area is the most sensitive variable to affect the system's performance. Therefore, in the analysis, the change of solar collector area is chosen as the driving parameters of the optimization. The economic Figure of merit used in the economic optimization is the payback period, as it shows how soon the initial investment can be returned by accumulated fuel savings [Kreider et al., 1989]. Other than the payback period, other economic Figures of merit commonly used in analyses are the annualized cost and the life cycle savings, as these two shows the costs and savings obtained from operating the system.

Within this Figure, several economic parameters are taken into account. These parameters include the life cycle of the system (n), fuel cost (C_F), fuel escalation rate (e), discount rate (i), and inflation rate (j).

4.4.1. Annualized Cost

Annualized cost is the yearly cost of the system, including the cost of auxiliary energy, maintenance, and operation. It is expressed as [Hawladar, 1987]:

$$C_A = C_S C_{RF}(i', n) + Q_A C_F \frac{C_{RF}(i', n)}{C_{RF}(i'', n)} + C_M + C_O \quad (4.46)$$

where C_A is the annualized cost, C_{RF} is the capital recovery factor, Q_A is the auxiliary energy consumption, C_M and C_O are maintenance and operation costs. It is important to notice that collector area related cost, C_S , is constructed of costs dependent and independent of collectors.

$$C_S = C_D A + C_I \quad (4.47)$$

Where

$$C_D = C_C + bC_T \quad (4.48)$$

Auxiliary energy is defined as the difference between energy demand and energy supplied by solar radiation.

$$Q_A = Q_D - Q_S \quad (4.49)$$

The capital recovery factor, C_{RF} , is defined as:

$$C_{RF} = \left\langle \left\{ \frac{1}{i} \left[1 - \left(\frac{1}{1+i} \right)^n \right] \right\}^{-1} \right\rangle \quad (4.50)$$

It can be seen that C_{RF} is a function of discount rates. Other than a regular discount rate, an effective discount rate and a fuel effective discount rate are also considered.

Effective discount rate is defined as:

$$i' = \left(\frac{i-j}{1+j} \right) \quad (4.51)$$

And, effective discount rate for fuel is defined as:

$$i'' = \left(\frac{i-e}{1+e} \right) \quad (4.52)$$

4.4.2. Life Cycle Savings

Life cycle savings is the difference between the life cycle cost of a system using conventional fuel only and life cycle cost of the solar energy system plus auxiliary energy cost. They are expressed by Hawlader [1987], as:

$$LCS = \frac{Q_S C_F}{C_{RF}(i'', n)} - C_S \quad (4.53)$$

4.4.3. Payback Period

Payback period is the minimum length of time needed for the system to be fully paid through the savings obtained from using solar energy. It is described by Hawlader [1987], as:

$$n_p = \frac{\ln[1 - (i-e)x_{pp}]}{\ln\left(\frac{1+e}{1+i}\right)} \quad (4.54)$$

Where x_{pp} is defined as:

$$x_{pp} = \frac{C_S + \frac{(C_M + C_O)}{C_{RF}(i', n)}}{Q_S C_F} \quad (4.55)$$

Chapter 5

RESULTS AND DISCUSSION

This chapter describes the experimental and simulation results of the study. Results of economic optimization are also presented. The main performance parameters are the collector efficiencies, distillate production rate, coefficient of performance (COP), and performance ratio (PR). The economic parameter to be observed is the payback period relative to the collector area and production rate.

For the purpose of experimental study, tap water is used in place of sea water. Comparison of experimental results for multi effect desalination system using seawater and tap water was presented by Rahman [2002], and it was concluded that, as far as distillation was concerned, there was no significant difference in results. The desalination chamber of the experimental system was based on the same principle of multi effect desalination.

5.1. Meteorological Condition of Singapore

Figures 5.1 and 5.2 show the values of solar radiation, wind speed, ambient temperature, and relative humidity of Singapore in January 2006. It can be seen that the temperature generally reaches around 30 °C, with the maximum value is at 35 °C and the lowest at around 27 °C. Wind speed varies from around 1 to 3 m/s, with relative humidity between 65 to 85%, and solar radiation varies from 400 to more than 1000 W/m². In general, the main characteristics of Singapore's climate are uniform ambient temperature, high humidity with frequent rainfall throughout the year (Hawlader et al., 1990).

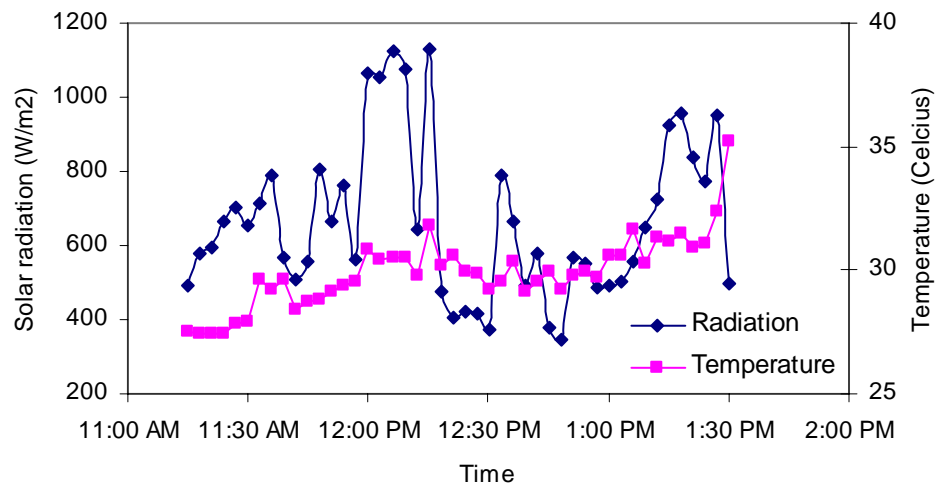


Figure 5.1. Values for solar radiation and ambient temperature in January 2006

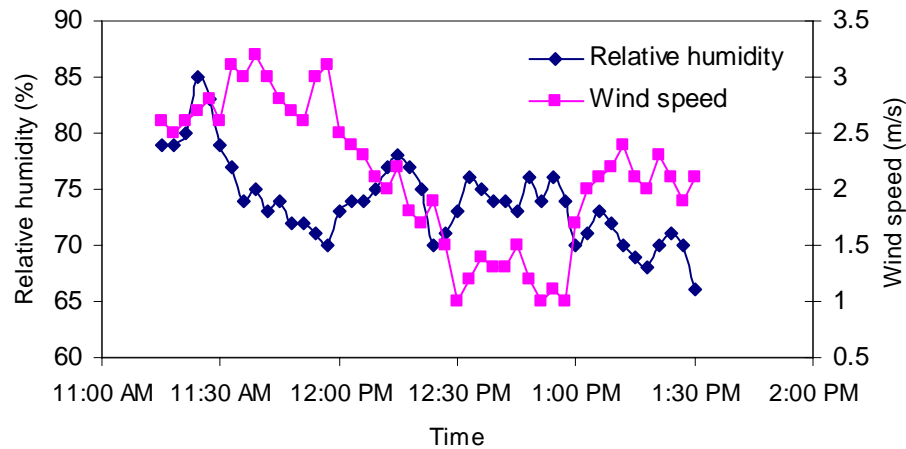


Figure 5.2. Values for relative humidity and wind speed in January 2006

5.2. Experimental Results

A series of experiments has been conducted on the solar assisted heat pump desalination system, under the meteorological conditions of Singapore. Influence of different parameters and the thermal performance of the system have been investigated and the results are presented in this section.

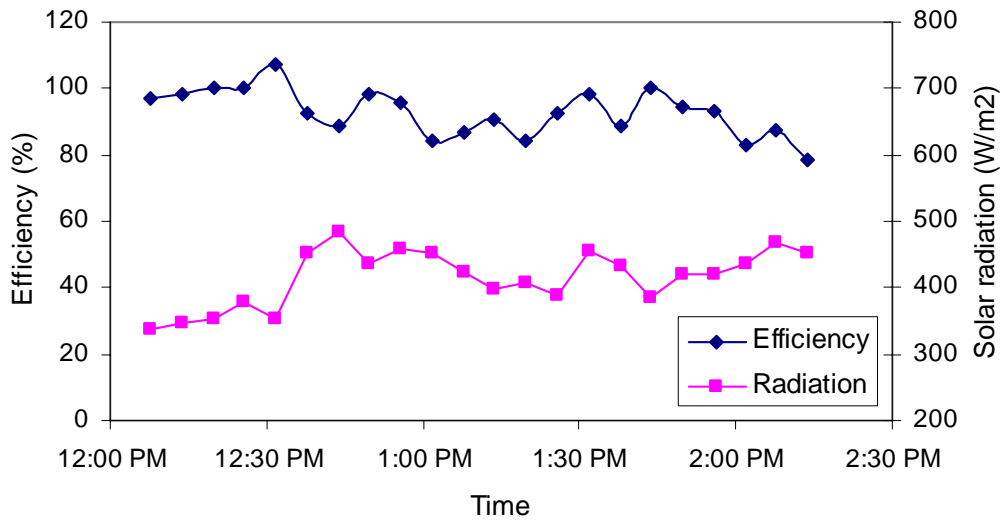


Figure 5.3 Change of evaporator collector efficiency and solar radiation with time

Figure 5.3 shows the change of evaporator collector efficiency with respect to time. The experiment was conducted in the month of December with the compressor speed at 30 Hz. Solar radiation was relatively stable during the course of the experiment. The efficiency of evaporator collector is sensitive to solar radiation. A low solar radiation will reduce the refrigerant temperature in the evaporator collector, leading to a lower heat loss from the collector and increased efficiency. In Figure 5.4 it can be seen that the ambient temperature of Singapore is relatively stable, with a temperature range of 28 to 31 °C at around noon. In general, the collector efficiency tends to have a value of 80 to around 100 percent.

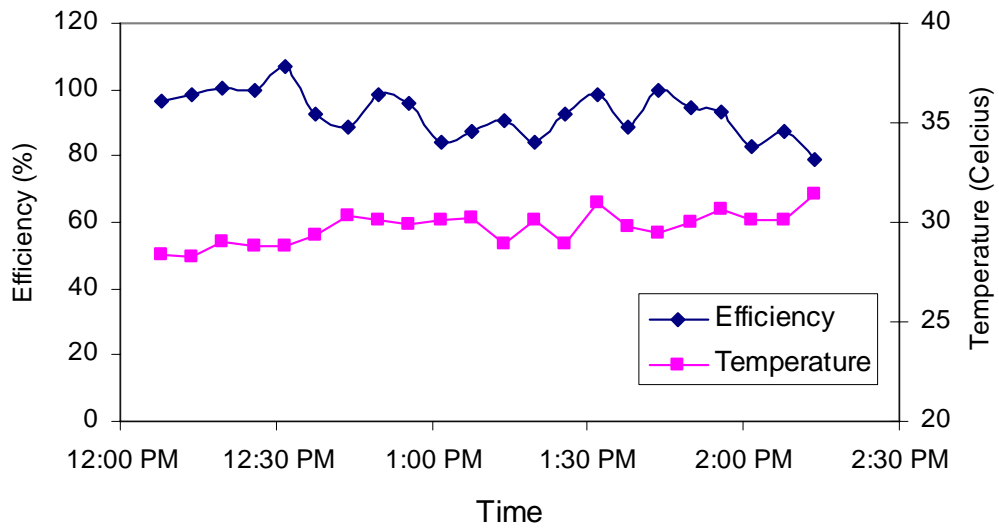


Figure 5.4 Change of evaporator efficiency and ambient temperature with time

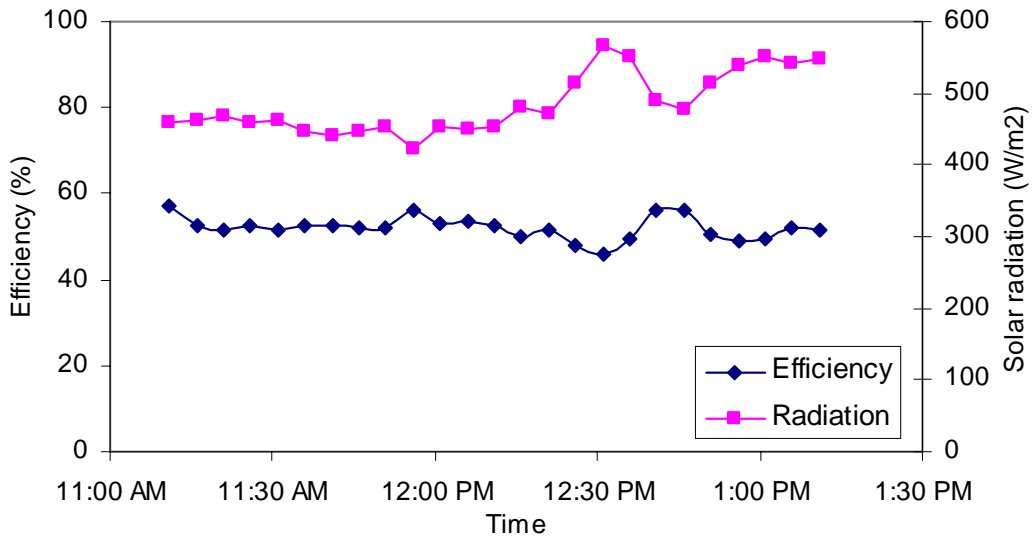


Figure 5.5 Change of liquid collector efficiency and solar radiation with time

The efficiency of the liquid solar collector is shown in Figure 5.5. It can be seen that at a relatively stable solar radiation, the collector efficiency is also stable. The collector, at 2 m², has an efficiency in the range of 50 to 60 percent.

Figure 5.6 shows liquid solar collector efficiency as a function of inlet water temperature and solar radiation. The $F_R(\tau\alpha)$ value is shown to be at 0.51. The slope of the line gives a value for $F_R U_L$ close to 2.94 W/m^2 , and a value of $U_L = 5.76 \text{ W/m}^2 \text{ K}$. Figure 5.7 shows the efficiency of evaporator collector. The $\tau\alpha$ value is close to unity. At $x = 0$, the F_R has a value close to 0.3. The slope of the line gives a value of $F_R U_L$ of $13.66 \text{ W/m}^2 \text{ K}$ and, hence, a value of $U_L = 45.5 \text{ W/m}^2 \text{ K}$.

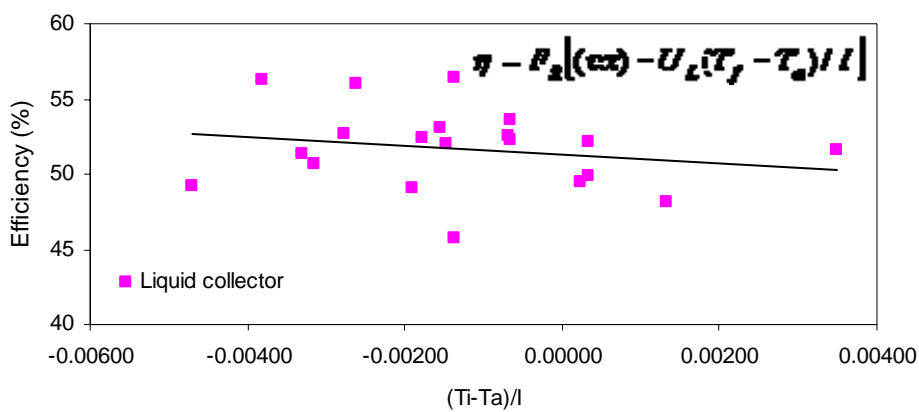


Figure 5.6. Liquid solar collector efficiency as a function of water inlet temperature and solar radiation

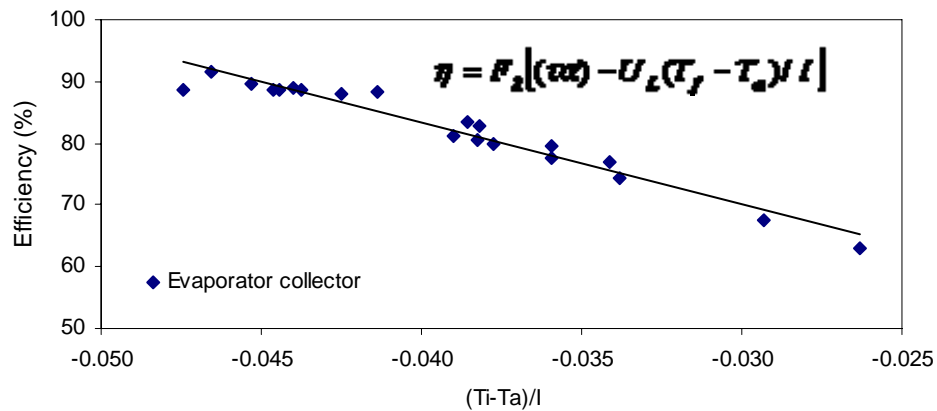


Figure 5.7. Evaporator collector efficiency as a function of refrigerant inlet temperature and solar radiation

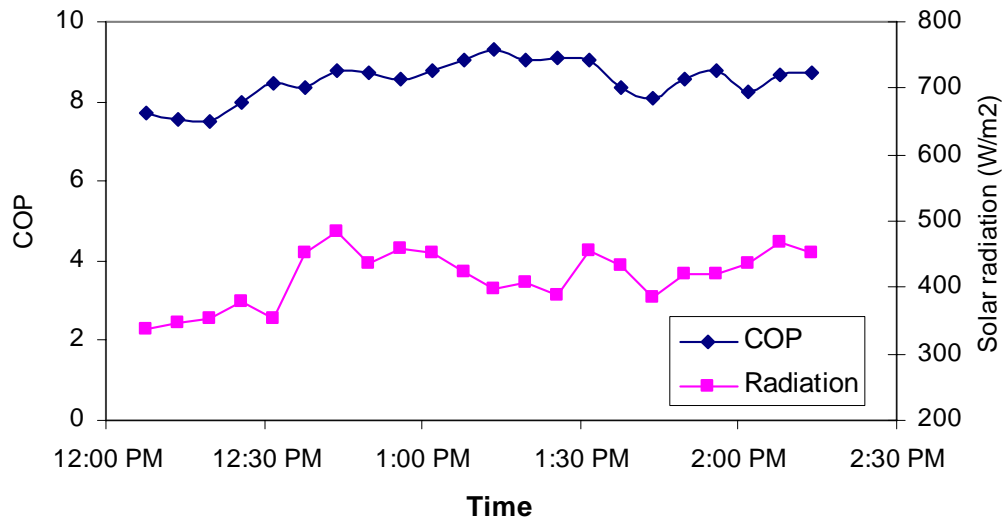


Figure 5.8. Change of COP and solar radiation with time

As shown in Figures 5.8 and 5.9, the coefficient of performance (COP) tends to have a relatively stable value. The relatively stable meteorological condition gives less fluctuation in the refrigerant temperature in the solar assisted heat pump, which leads to a more stable value of the COP. The COP has a value in the range of 8 to 9. During the experiment the ambient temperature was relatively stable, with a value close to 30 °C and the solar radiation varies from 300 to 500 W/m².

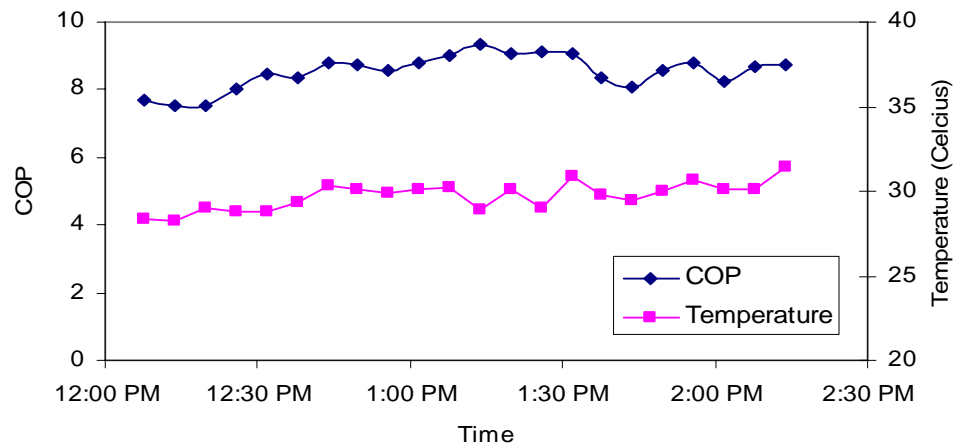


Figure 5.9. Change of COP and ambient temperature with time

Water production rate is measured every 30 minutes. From Figures 5.10 and 5.11, it can be seen that the maximum water production rate is close to 0.9 kg/hr. The performance ratio is a function of water production rate, thus the change of production rate will affect the performance ratio. From Figure 5.10, the performance ratio is shown to be close to 1.5. Figure 5.11 shows a comparison of the production rate and the average solar radiation value during the 30 minutes interval of collection. It can be seen that the production rate tends to follow the solar radiation value. The amount of water that undergoes thermodynamic flashing depends on how much heat they absorb from solar radiation. Thus the production rate will be affected by the solar radiation.

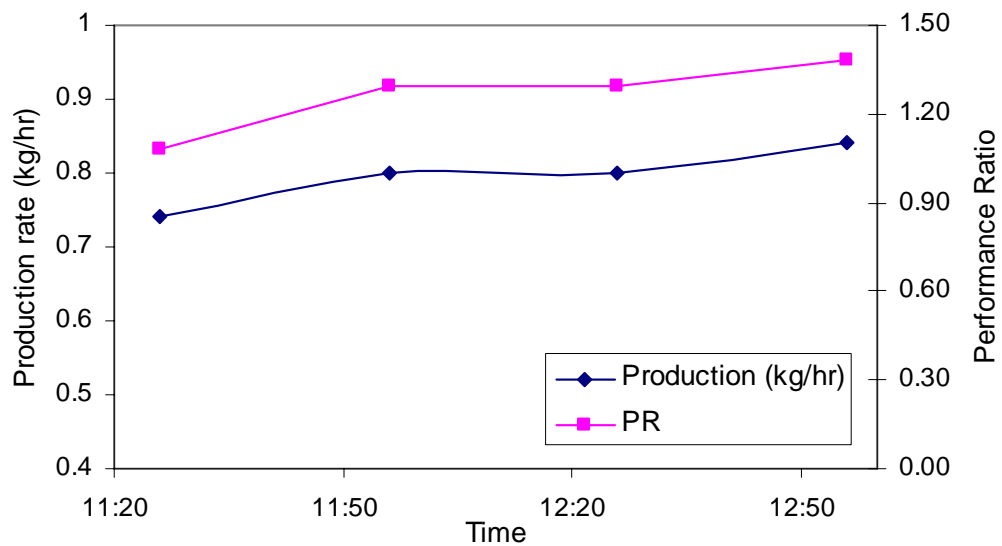


Figure 5.10 Water production rate and performance ratio

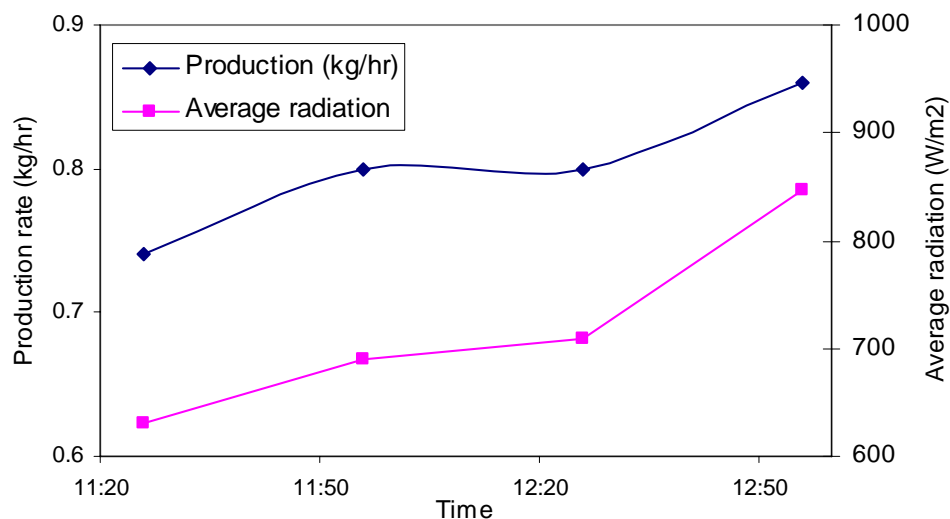


Figure 5.11 Comparison of water production rate and average solar radiation

It can be seen that the solar radiation greatly affects the performance of the system. The following section will observe the general trend of how the system behaves as solar radiation increases.

The COP readings obtained for the compressor speed of 30 Hz is shown in Figure 5.12. It can be seen that the COP value tends to rise as the solar radiation increases. This is due to the refrigerant absorbing more heat at higher radiation, causing more heat to be released in the condenser coil. It can be seen that the highest COP value reached around 10, while the lowest is close 6. In general, the COP of the system lies between 8 and 10.

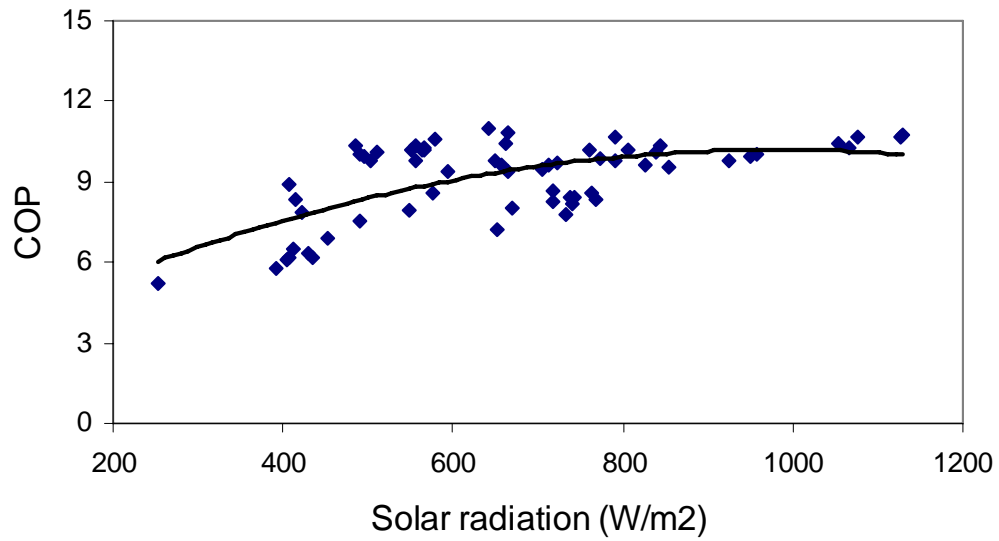


Figure 5.12 Change of COP to Solar radiation

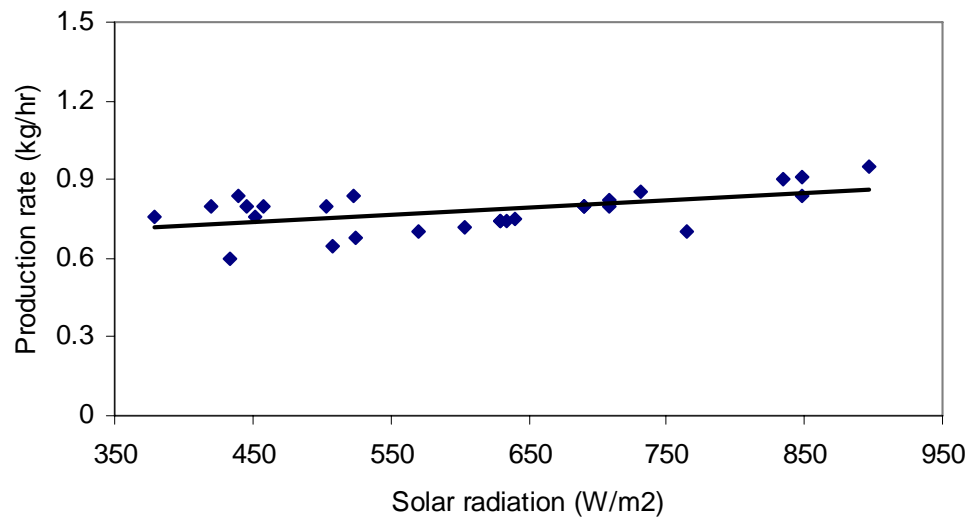


Figure 5.13 Effect of solar radiation to production rate

In Figure 5.13, the increase of solar radiation resulted in higher production rate. With higher solar radiation, more vapors are produced in thermodynamic flashing. It can be seen that the production rate varies from 0.6 to close to 1 kg/hr.

5.3. Comparison of Experimental and Simulation Results

The meteorological condition for the day during the experiment conducted in December is shown in Figure 5.14. It can be seen that the ambient temperature is relatively constant with a value close to 30 °C. The maximum solar radiation value reaches around 1000 W/m², and it varies throughout the measurement with the lowest value reaches around 400 W/m²

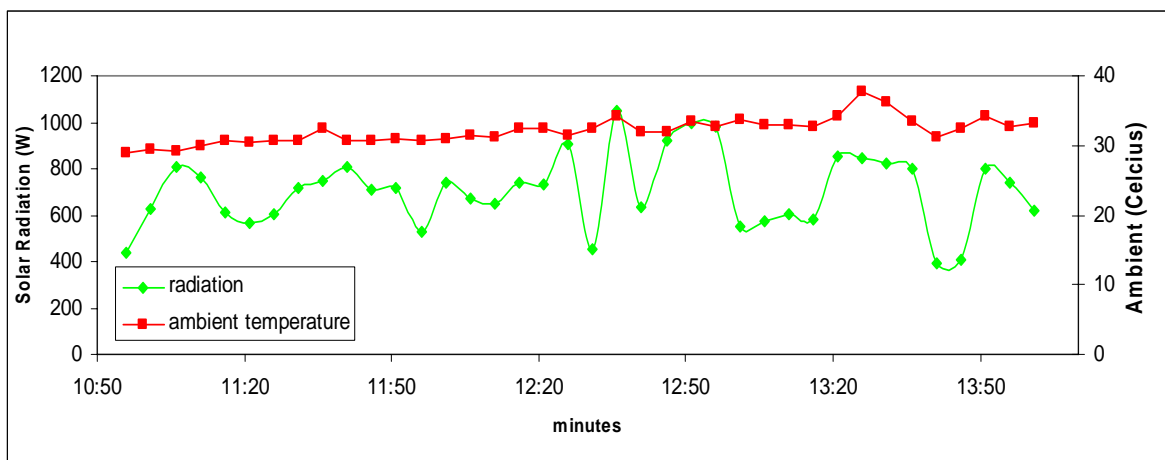


Figure 5.14 Solar radiation and ambient temperature for a day in December

Figure 5.15 shows the comparison of simulation and experimental results plotted against time. As can be seen from the Figure, there is a good agreement between the two results. Liquid collector efficiency varies between 40 to 60%. Higher efficiency value occurs during low solar radiation, where less heat loss occurs.

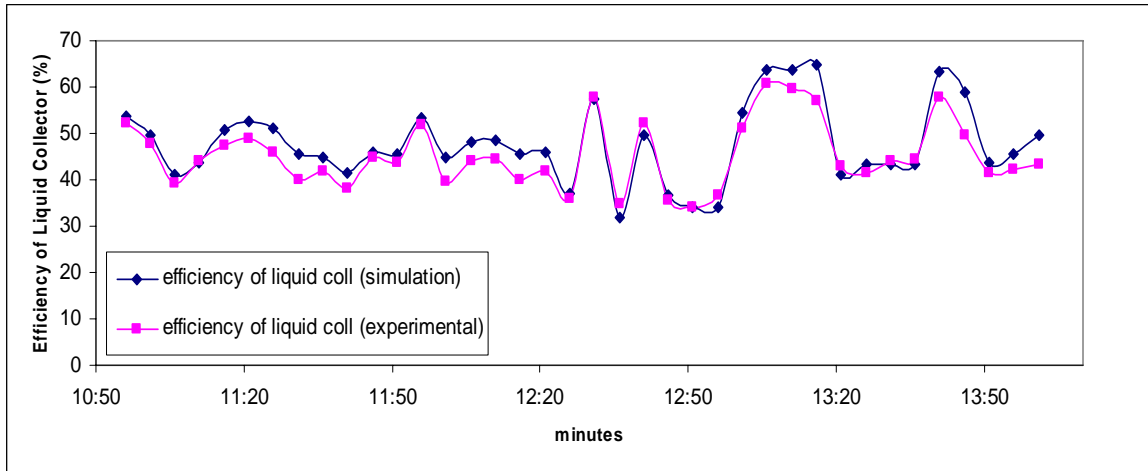


Figure 5.15 Comparison of simulated and experimental result of liquid collector efficiency

Comparison between simulated and experimental results of evaporator collector efficiency is shown in Figure 5.16. Compared to the liquid collector, the evaporator collector has a higher efficiency value. This is due to the evaporator collector operating at a temperature lower than the ambient, thus enables it to absorb heat both from the ambient air and solar radiation. From the Figure, it can be seen that evaporator collector efficiency may reach higher than 80% due to its low operating temperature.

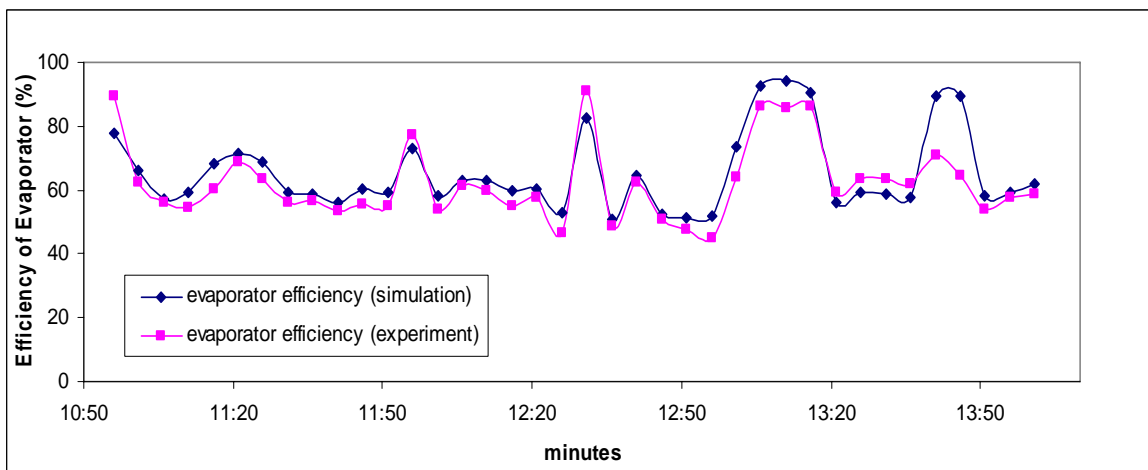


Figure 5.16 Comparison of simulated and experimental result of evaporator collector efficiency

Figure 5.17 shows the comparison of experimental and simulated COP values, with the compressor running at 30 Hz. The highest COP value, for both simulation and experiment, reaches around 10, while the lowest is around 6. Higher COP values took place at higher solar radiation value.

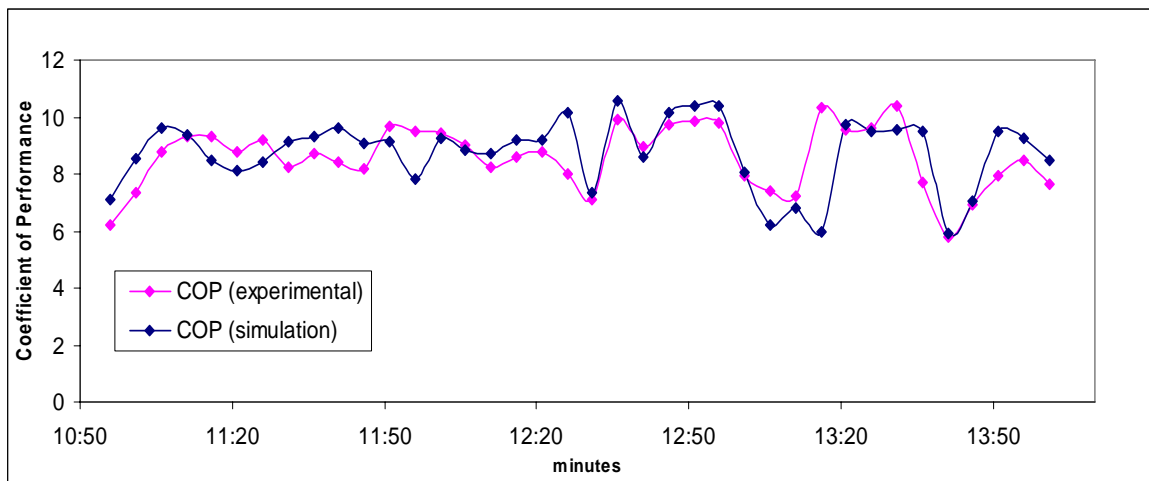


Figure 5.17 Comparison of simulated and experimental result of COP

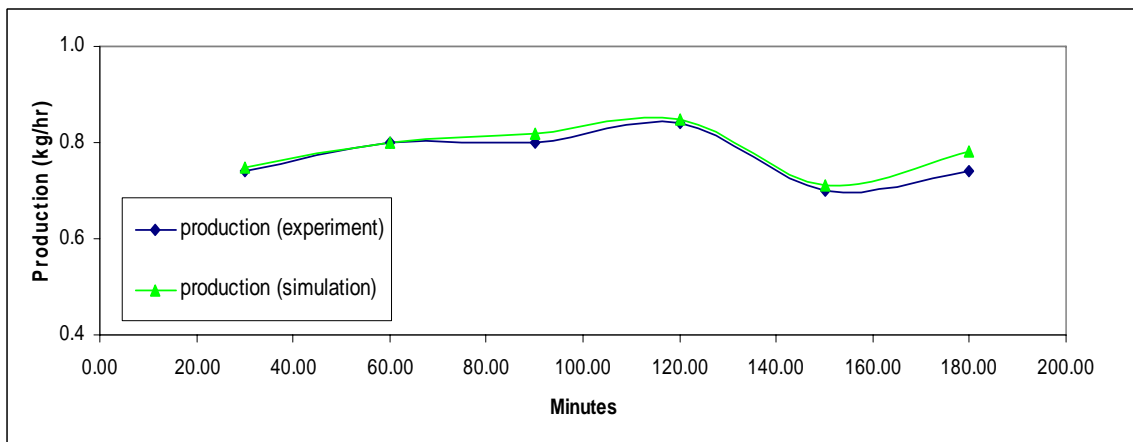


Figure 5.18 Comparison of simulated and experimental result of water production

Figure 5.18 shows the water production rate of the system. The average production rate was shown to be close to 0.8 kg/hour. At higher solar radiation, the system yields more water. This is caused by the feed water absorbing more heat, thus more vapors are

produced in thermodynamic flashing. The value of Performance Ratio is dependent upon the water production rate, thus it shows similar variation with the production rate. As can be seen from Figure 5.19 the Performance Ratio reaches close to 1.2.

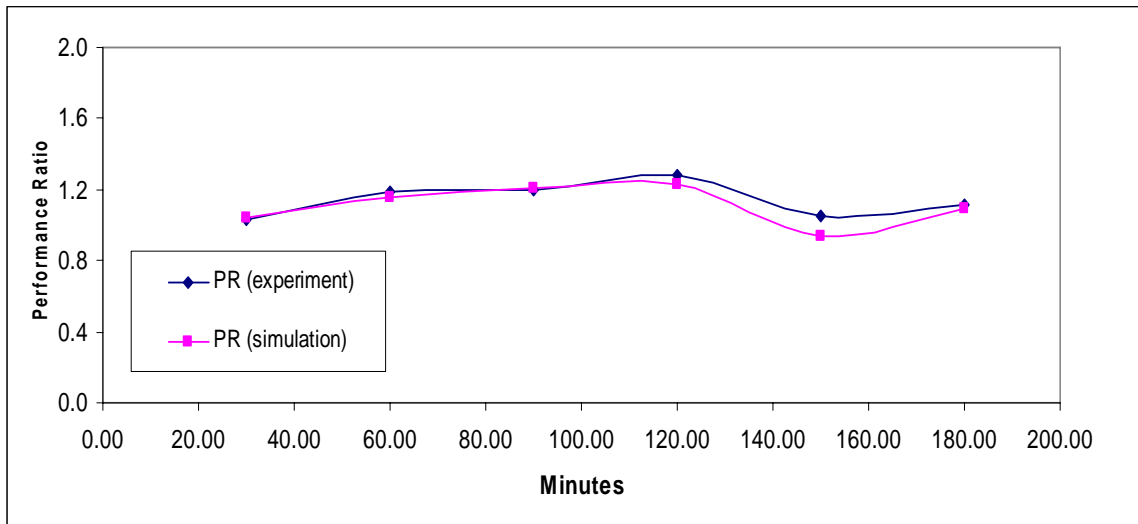


Figure 5.19 Comparison of simulated and experimental result of Performance Ratio

5.4. Results of Parametric Study

Results of the parametric study are presented here. The study observes the parameters affecting the production rate. The parameters taken into account are the temperature of the feed water entering the distillation chamber, solar radiation, ambient temperature, operating frequency of the compressor, and the pressure within the distillation chamber.

Figure 5.20 shows the effect of feed water temperature leaving the liquid collector on production rate, and the corresponding collector area. Variation of results is taken for solar radiation at 300 W/m^2 and 600 W/m^2 . The ambient temperature is set at $29 \text{ }^\circ\text{C}$, with the running frequency at 30 Hz . From the Figure, it can be seen that increase of feed temperature has a positive effect on production rate. This is due to the fact at higher

temperature, feed water will be able to produce more vapor in thermodynamic flashing. Consequently, at a constant radiation value, a higher feed water outlet temperature will require more heat from solar radiation and, thus increased the liquid collector area. From the Figure, assuming a constant solar radiation value, it can also be seen that at higher solar radiation, as the source of heat, increases the production rate. At high solar radiation less collector area is needed to heat the feed water compared to a lower solar radiation value.

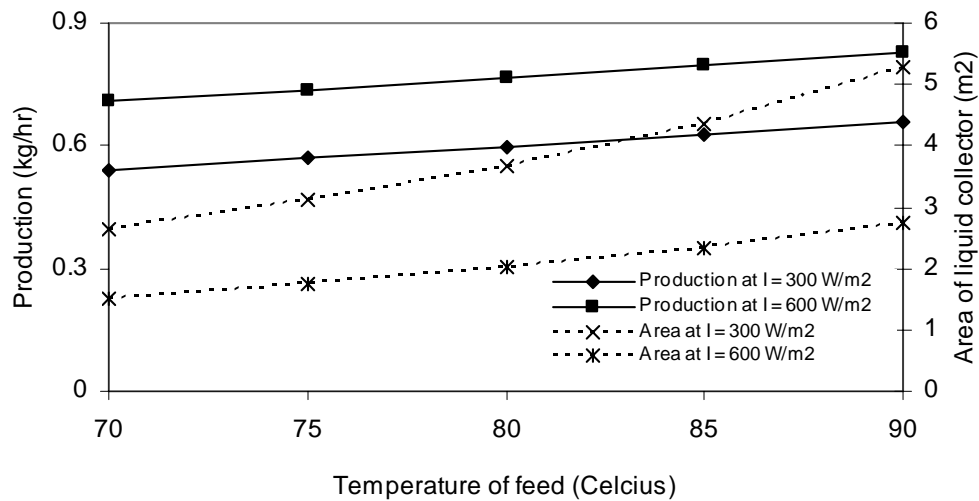


Figure 5.20 Effect of feed temperature to production rate and liquid collector area

Effect of solar radiation on production rate and liquid collector efficiency is shown in Figure 5.21. From the Figure, it can be seen that at higher radiation value, and a constant collector area, the efficiency of the collector is reduced due to the larger difference of feed water temperature to that of the ambient, thus causing more heat loss. However, increase of solar radiation has a positive effect to production rate, as higher solar radiation causes feed water to release more heat in thermodynamic flashing. A change of ambient temperature does not have much effect to the collector's efficiency and production rate.

However, a drop in ambient temperature does give a negative effect on both parameters. A drop in temperature will increase the heat loss of the collector, causing it to lose its efficiency, and reducing the amount of heat available for flashing.

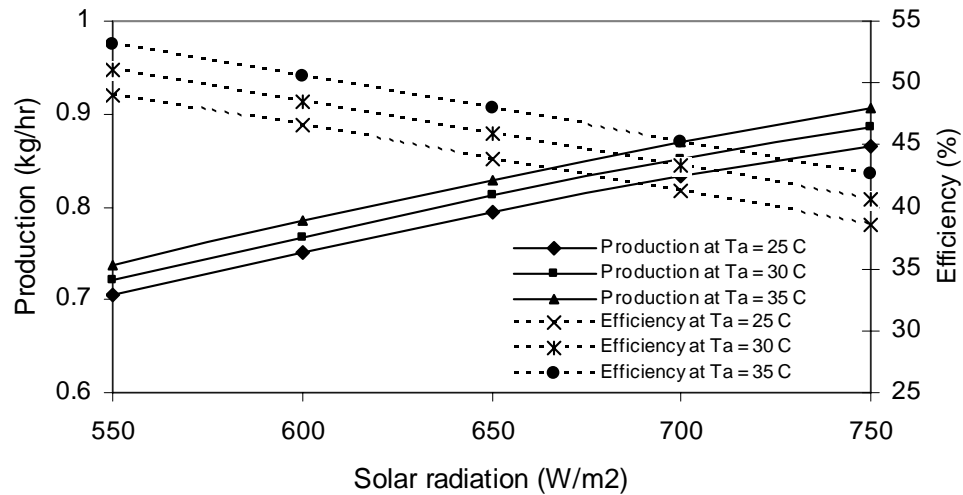


Figure 5.21 Effects of solar radiation on production rate and liquid collector efficiency

A further observation of the increase of ambient temperature is shown in Figure 5.22. Keeping solar radiation at 600 W/m^2 , it can be seen that an increase of ambient temperature contributes to an increase of feed temperature and production rate. With a higher ambient temperature, the liquid solar collector loses less heat to the environment, thus providing a higher feed water temperature and producing more vapor in thermodynamic flashing. The effect of distillation chamber pressures to production rate is shown in Figure 5.23. With the compressor running frequency at 30 Hz, the increase of vacuum pressure inside the chamber will result in higher production rate. At a higher pressure, less latent heat is needed to evaporate saturated water thus contributing to the increase of production rate.

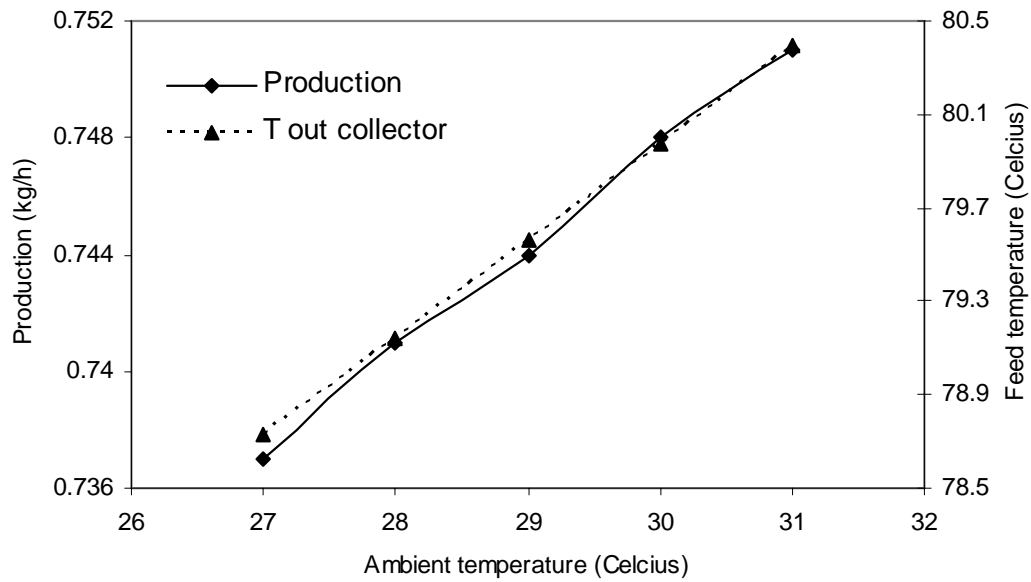


Figure 5.22 Effect of ambient temperature to production rate and feed temperature ($I = 600 \text{ W/m}^2$, chamber pressure at 0.14 bar)

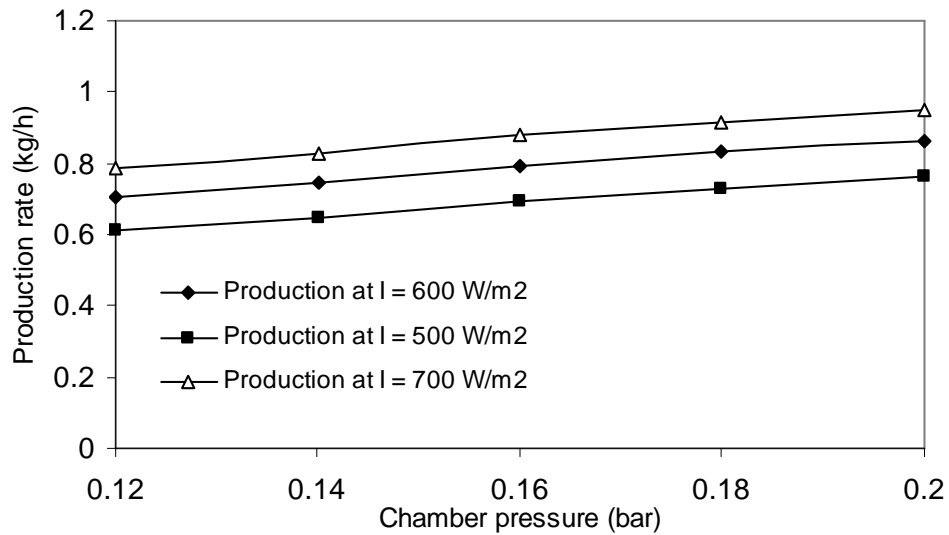


Figure 5.23 Effect of chamber pressure to production rate

Figure 5.24 shows the effect of solar radiation on outlet temperature of evaporator collector and production rate. Increase of solar radiation has a desirable effect to the production rate and outlet temperature. At higher radiation values, the evaporator collector

absorbs more energy, delivering more heat to evaporate saturated water in the chamber. The increase of collector temperature is thus followed by an increase of production rate.

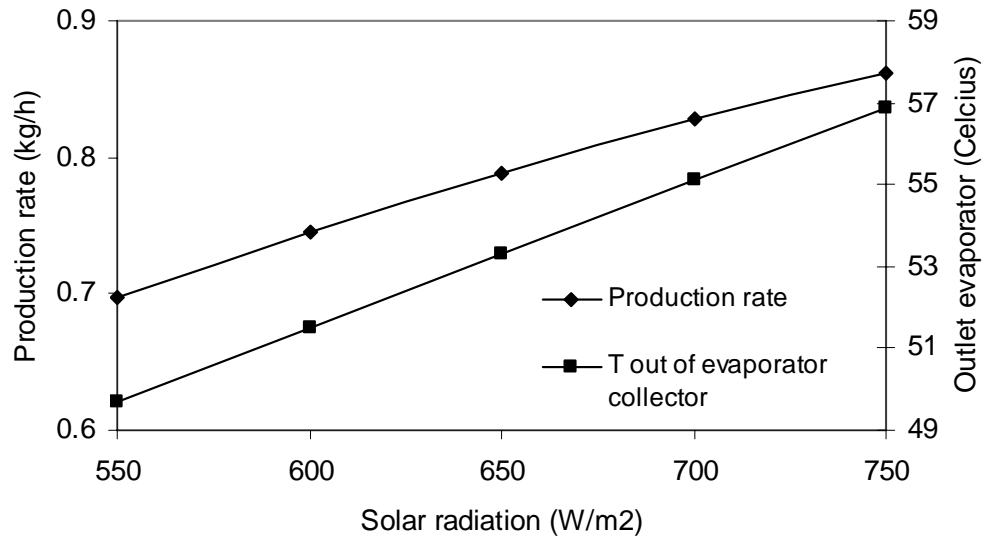


Figure 5.24 Effect of solar radiation to evaporator outlet temperature and production rate

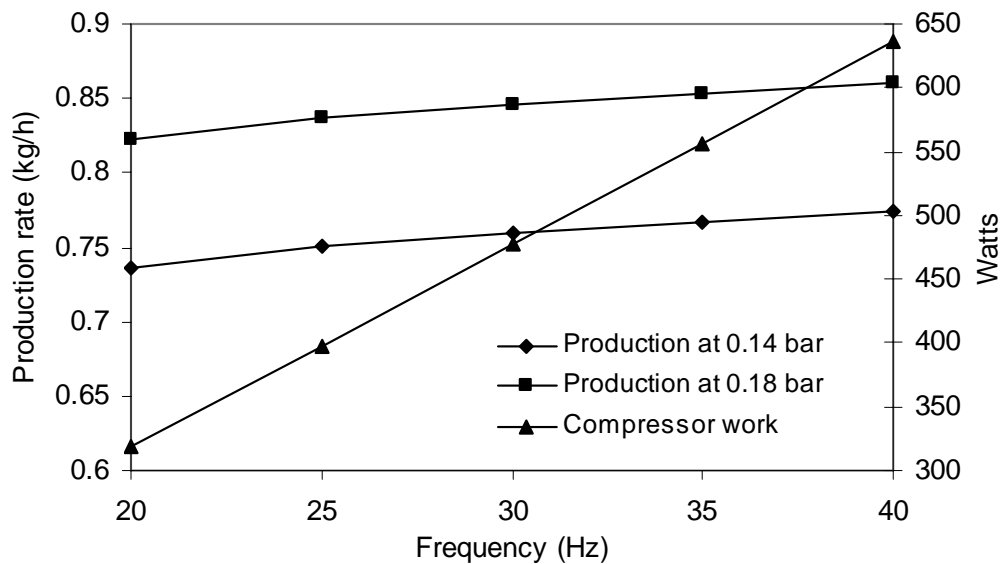


Figure 5.25. Effect of compressor running frequency to production rate and electricity consumption

An increase of compressor running frequency corresponds to larger electricity consumption, as shown in Figure 5.25. With a constant solar radiation of 600 W/m², the

increase of frequency compresses the refrigerant into a higher energy state, resulting in an increase of production rate due to more heat being released in the chamber.

5.5. Results of economic optimization

The principal reason for using solar energy in a thermal process, other than the environmental considerations, is to reduce the energy cost normally associated with the burning of fossil fuel to produce heat. Therefore, an economic optimization is needed to determine the feasibility of a solar thermal system in terms of its return on investment.

Installations of solar thermal systems are usually marked with a high initial investment cost and a low operating and energy cost. The increase of a system's energy demand is usually followed by an increase of the solar collector's area. Thus the collector area is the most influential parameter in determining the return on investment (payback period) of the system.

Results of economic optimization are presented in this section. Table 5.1 shows the economic parameters used in calculating the payback period. Further analyses of these parameters are also presented. The costs of solar energy and heat pump systems are influenced heavily by the collector cost per unit area and compressor cost. Thus, for the proposed solar heat pump desalination system the payback period is calculated with regard to the optimum collector area with a different compressor cost for various production rates.

Life cycle of the system (n)	20 years
Fuel cost (C_F)	S\$0.06/MJ
Fuel price escalation rate (e)	3%
Discount rate (i)	7%
Inflation rate (j)	1.4%
Liquid collector cost	S\$420/m ²
Evaporator collector cost	S\$250/m ²
Condenser tank cost per collector area	S\$350/m ²
Maintenance and operation cost	10% of collector cost

The solar assisted heat pump desalination system, which has been constructed, is an experimental setup, thus it produces a small amount of desalinated water. In order to make it economically feasible, it is necessary to scale up the system into a higher production capacity, one that is able to provide water for domestic needs, or to supply water in remote areas. From Table 5.2, we can see that to supply the water requirement for a single family we need to produce at least more than 150 *l* of water per day. With a production rate of 150 *l*/day, the system will also be able to supply potable water to a remote elementary school of 60 students. However, we must always take into account the amount of investment needed and the payback period of the system to make it economically feasible.

Table 5.2 Water requirement of commercial and institutional buildings [Stein et al, 1986]

Type of Building	Average water consumption per day
Men's dormitories	50 l/student
Women's dormitories	45 l/student
Motels:	
60 units	55 l/unit
100 units or more	40 l/unit
Office buildings	4 l/person
Nursing homes	70 l/bed
Apartment houses:	
50 units	152 l/units
100 units	140 l/units
200 units	133 l/units
Schools:	
Elementary	2.5 l/student
Junior and senior	7 l/student

A high price of solar collector will cause the solar energy savings to be less competitive compared to conventional fuel systems. Therefore, other than using solar thermal energy, it is necessary to make use of the heating and cooling provided by the heat pump efficiently. In order to achieve this, a new setup is proposed as shown in Figure 5.26. In the new setup, the refrigerant is allowed to condense fully through the distillation chamber and water tank, thus heating the feed water. Therefore, the need of liquid solar collector to preheat the feed water may be removed from the system. In the new design, the distillation chamber will maintain the same vacuum pressure of 0.14 bar, thus water saturation temperature will still be at 52 °C. Refrigerant leaving the chamber will preheat the feed water tank to be close to 50 °C, thus reducing the need of condenser tank, and water will be heated further by the electrical heater to 70 °C. The evaporator collector will heat the refrigerant until 50 °C, and the compressor will further increase its energy level to 70 °C.

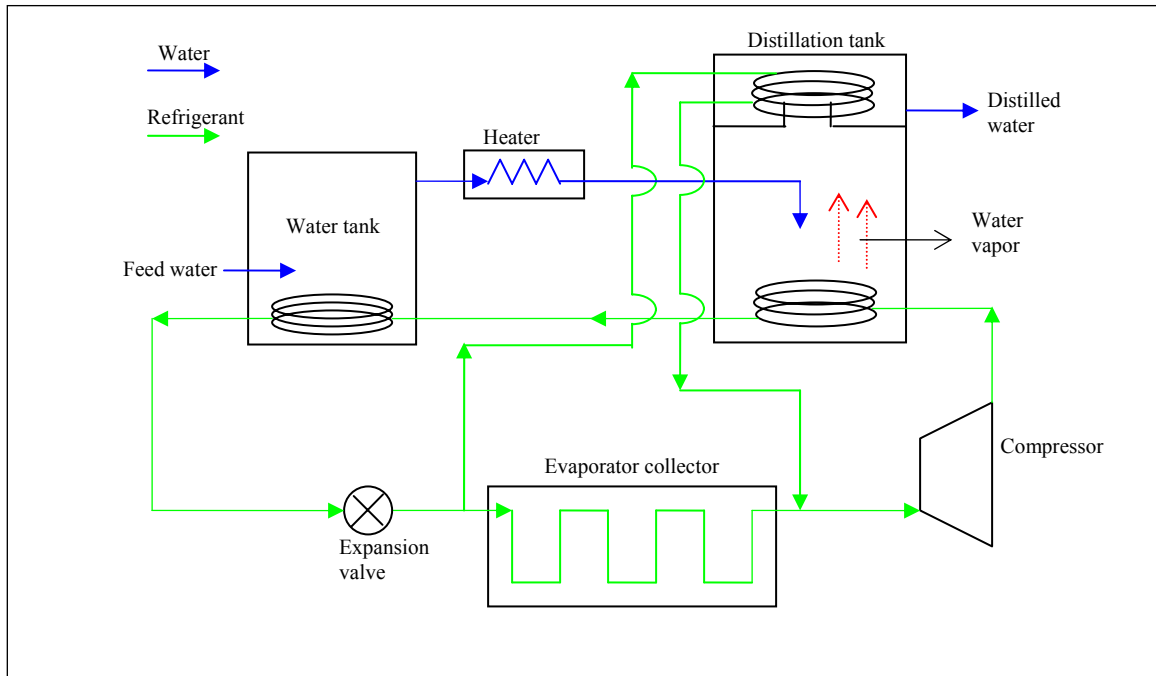


Figure 5.26 Proposed solar heat pump desalination setup

The proposed setup produces distillate water at different production rates, and thus different component sizes and investments are needed. A comparison of the production rates, 225 l/day, 450 l/day, and 900 l/day showed that at lower production rate, the payback period increases. At low production rate, as shown in Figure 5.27, less solar energy is used in the process, thus the fuel savings is reduced, resulting in higher payback period. At 225 l/day the payback period is close to 4 years, while at 450 and 900 l/day the optimum payback period close to 3.5 years. At 900 l/day, the operation and maintenance cost of the system is high, thus reducing the savings acquired from solar energy usage, causing a similar payback period to 450 l/day. At 225 l/day the optimum collector area is 20 m², while for 450 and 900 l/day it is 34 and 67 m², respectively. For production of 450 l/day, it is achieved with a compressor power input of 15 kW, and 30 kW for 900 l/day.

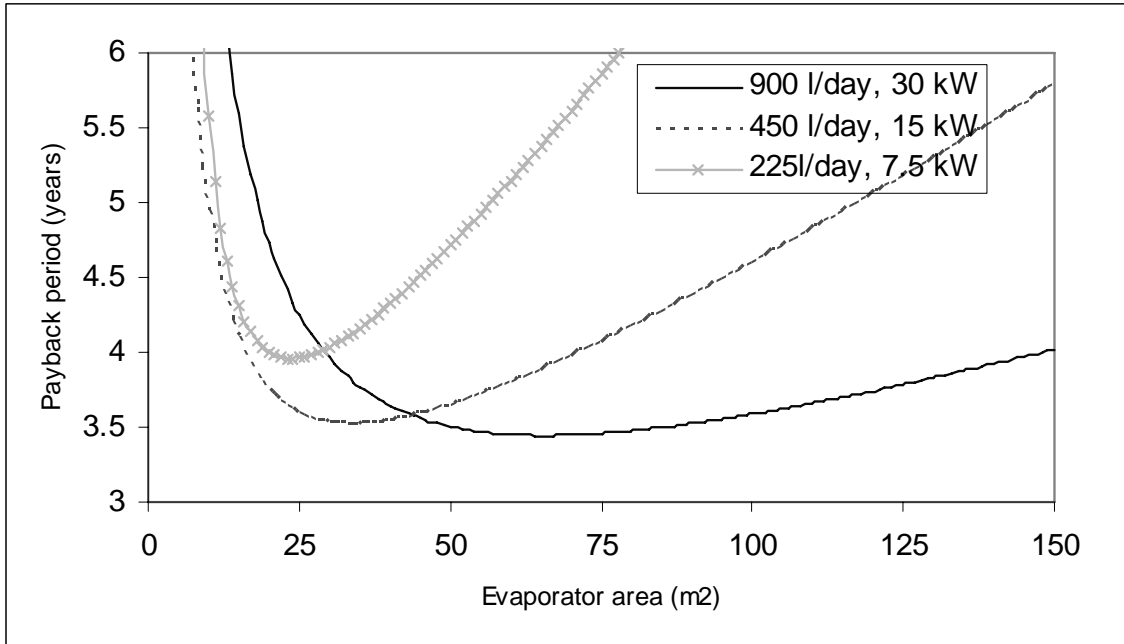


Figure 5.27 Comparison of payback period for different production rates

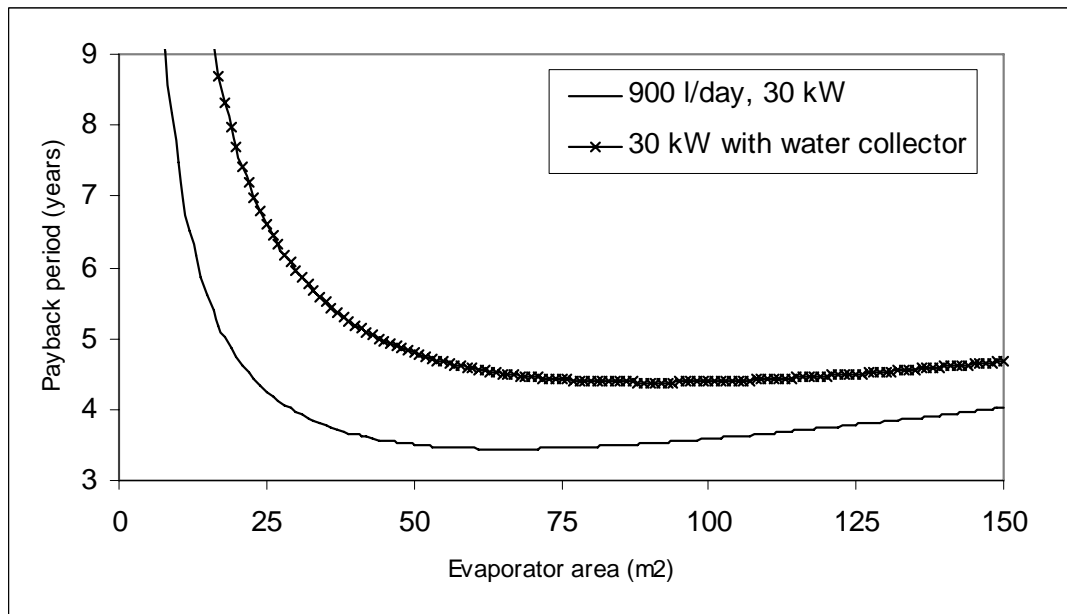


Figure 5.28 Comparison of payback period with the usage of liquid solar collector

As shown in Figure 5.28, installation of solar water collector to the system with a production rate of 900 l/day will increase its optimum payback period to more than 4

years. A system with the same production rate will have a lower payback period without utilizing the solar water collector.

Further analysis for the production of 900 l/day is shown in Figure 5.29. It can be seen that a variation of inflation rate (j) and fuel escalation rate (e) does not have much effect on the payback period. The variation of discount rate (i) gives a more significant effect, but it is the price of fuel (C_F) that will greatly affect the payback period.

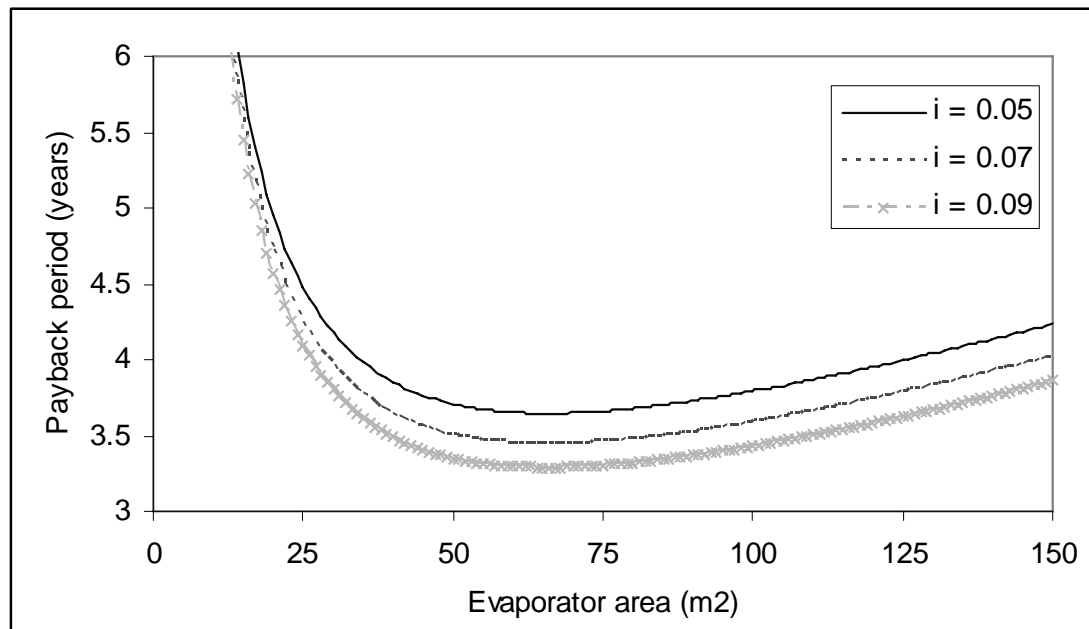


Figure 5.29 Effect of discount rate (Production rate: 900 l/day)

The increase of discount rate (i) will reduce the payback period, as shown in Figure 5.29. The discount rate shows the future value of the investment relative to the current value. Thus, a higher discount rate means a higher return value of investment in the future, which

resulted in a higher energy cost savings. Figure 5.29 showed that for a discount rate close to 0.1, the payback period of the system will be less than 3.5 years.

The effect of inflation is shown in Figure 5.30. It can be seen that a little change in inflation will not have much effect in payback period either. For an inflation rate of around 1%, the payback period of the system is close to 3.5 years. The change in fuel escalation rate will also cause a little change in payback period, as shown in Figure 5.31. A 5% change of fuel escalation rate, from 3% to 8%, will slightly reduce the payback period to less than 3.5 years.

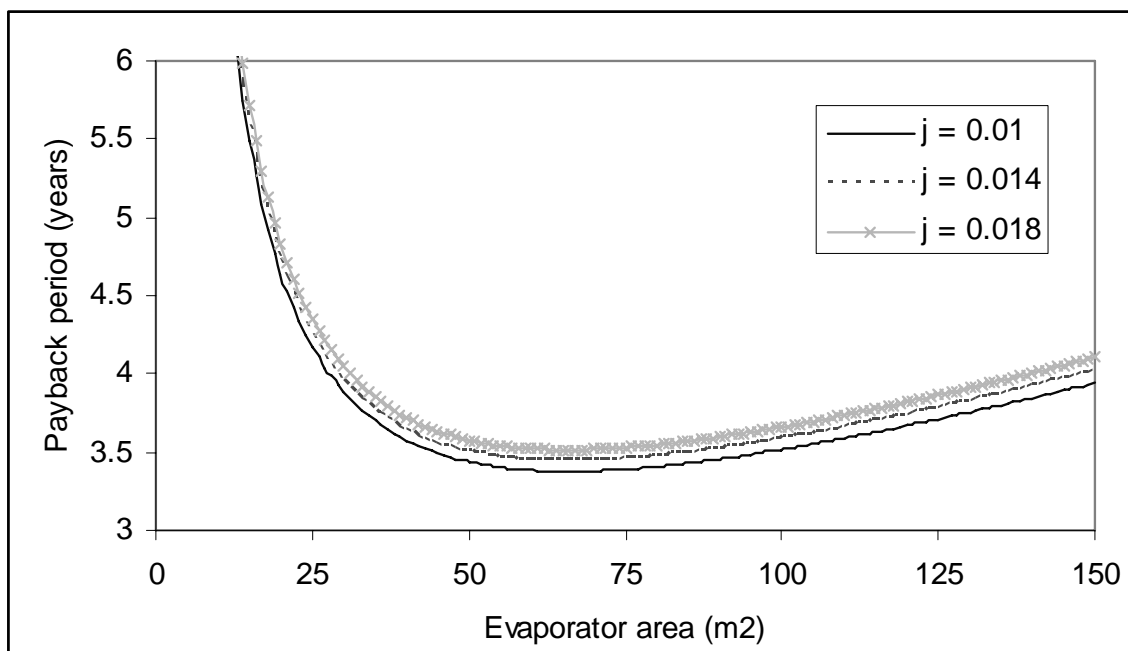


Figure 5.30 Effect of inflation rate (Production rate: 900 l/day)

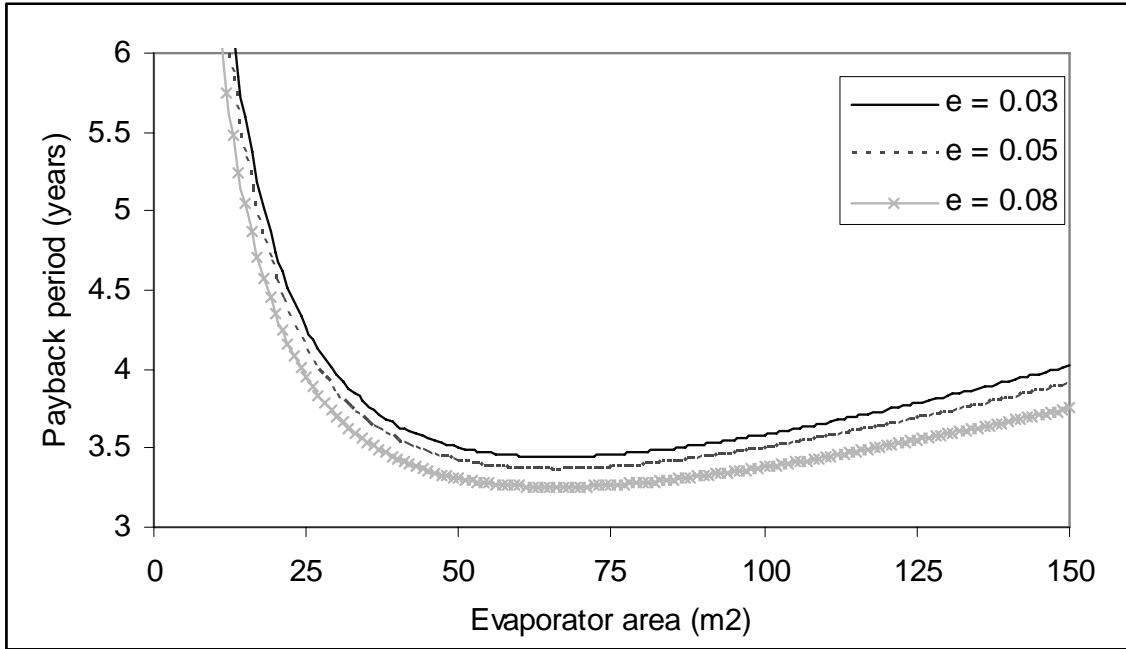


Figure 5.31 Effect of fuel escalation rate (Production rate: 900 l/day)

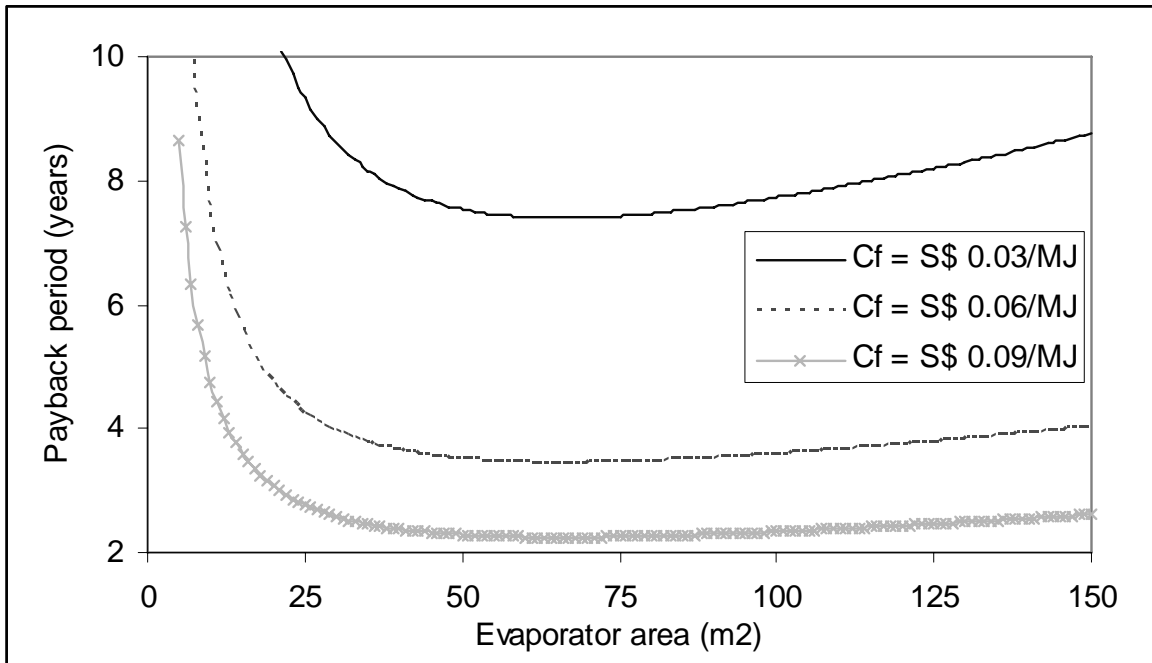


Figure 5.32 Effect of fuel price (Production rate: 900 l/day)

The most influential economic parameter to the payback period is the fossil fuel price, as can be seen in Figure 5.32. A slight increase of the fuel price will reduce the payback period significantly. Thus if the oil price continues to increase in the future, solar energy will become a very competitive source of energy. At S\$ 0.09/MJ (S\$ 2.88/l) the payback period will be close to 2 years.

Chapter 6

CONCLUSIONS

A series of experiments has been conducted with the solar assisted heat pump desalination system. A liquid solar collector was added to the system to preheat the feed water before entering the distillation chamber. Experimental results showed that the system could reach a Coefficient of Performance (COP) of 10, and at a relatively stable meteorological conditions, the evaporator collector has an efficiency value between 80 and 90%, whereas the liquid solar collector has an efficiency value between 50 and 60%. The water production rate is generally close to 1 l/hr for the system, with a Performance Ratio (PR) close to 1.5.

A mathematical model of the system and a simulation program were then constructed to analyze the performance of the system. Comparison of simulation and experimental results showed good agreement, and indicates that the program is able to predict the performance of the system at a given meteorological condition. A parametric study of the system was then conducted using the program to further analyze the behavior of the system. Parametric study showed that increasing the feed temperature and reduction of chamber pressure has increased the production rate. However, an increase of solar radiation will reduce the efficiency of the collectors, as the increase of the refrigerant and feed water temperatures will increase the heat losses as well.

An economic analysis was conducted to determine the feasibility of the system. It was found out that in order to be feasible, the system's production capacity must be increased.

However, the increase of production rate will also increase the investment cost of the system. With the high price of liquid solar collector, the payback period of the system becomes less feasible. A new design of the system, one that does not use liquid solar collector, was proposed. With the new design, the payback period of the system becomes much more attractive. A high production rate will require more investment cost, and it is shown that removing the liquid solar collector will reduce the payback period significantly. The optimum payback period of the system with a 900 l/day production is close to 3.5 years with a 67 m² evaporator collector. Analysis of the economic parameters showed that the oil price is very influential in determining the competitiveness of the system.

In conclusion, it was found that the solar assisted heat pump desalination system exhibits great potential for future developments. With the increase of oil fuel prices, solar energy will likely to be more economically feasible as a source of clean energy.

Chapter 7

RECOMMENDATIONS

The system was built to operate on an experimental scale. To give a more realistic experimental result, one that which could provide water for domestic scale, it will be more beneficial if the existing system is modified, increased in terms of its production capacity, to meet this need.

As shown in the previous chapter, to reduce the investment cost of the system, the liquid solar collector may be removed from the system. To fully condensate the refrigerant, and at the same time, preheating the feed water, the feed water tank might be used as a condenser for the solar assisted heat pump. Such configuration will reduce the complexity of the system and reduces heat loss.

Other method to make use of the heat released by the solar assisted heat pump, is by implementing a second distillation chamber to allow further heat extraction from the condenser coils. This way, the method will also increase the production rate of the system.

REFERENCES

- Al-Kharabsheh, S. and D. Yogi Goswami, 2004, Theoretical Analysis of A Water Desalination System Using Low Grade Solar Heat. *Journal of Solar Energy Engineering*, Vol. 126, pp. 774-780
- Bahar, Rubina, M.N.A. Hawlader and Liang Song Woei, 2004, Performance Evaluation of a Mechanical Vapor Compression System. *Desalination*, vol. 166 pp 123-127
- Becker, Martin, 1986, *Heat Transfer: A Modern Approach*, Plenum Press, New York
- Bohner, A., 1989, Solar Desalination with A High Efficiency Multi Effect Process Offers New Facilities. *Desalination*, Vol. 73, pp. 197-203
- Brown, Royce N., 2005, *Compressors: Selection and Sizing*, Elsevier
- Chaturvedi, S.K., Y.F. Chiang and A.S. Roberts, Jr., 1982, Analysis of Two Phase Flow Solar Collectors with Application to Heat Pumps. *Journal of Solar Energy Engineering*, Vol. 104, pp. 358-365
- Duffie, John A. and William A. Beckman, 1980, *Solar Engineering of Thermal Processes*. John Wiley and Sons
- Dvornikov, Victor, 2000, Seawater multi effect distillation energized by a combustion turbine. *Desalination*, vol. 127 pp 261-269
- El-Dessouky, Hisham, Hisham Ettouney and Yosef Al-Roumi, 1999, Multi-Stage Flash Desalination: Present and Future Outlook. *Chemical Engineering Journal*, vol. 73 pp 173-190
- El-Nashar, Ali M., 2000a, Economics of Small Solar-Assisted Multiple Effect Stack Distillation Plants. *Desalination*, Vol. 130, pp. 201-215
- El-Nashar, Ali M., 2000b, Validating the Performance Simulation Program SOLDES Using Data From An Operating Solar Desalination Plant. *Desalination*, Vol. 130, pp. 235-253
- Fiorenza, G., V.K. Sharma and G. Braccio, 2003, Thermo-Economic Evaluation of A Solar Powered Water Desalination Plant. *Energy Conversion and Management*, Vol. 44, pp. 2217-2240
- Hawlader, M.N.A., K.C. Ng, T.T. Chandratilleke, D. Sharma and Kelvin Koay H.L., 1987, Economic Evaluation of A Solar Water Heating System. *Energy Conversion Management*, vol. 27, pp 197 – 204

- Hawladar, M.N.A, T.Y. Bong, and Wan Mahmood, 1990, Some Frequently Used Meteorological Data for Singapore, *International Journal of Solar Energy*, Vol. 8, pp 1-11
- Hawladar, M.N.A., Prasanta K. Dey, Sufyan Diab and Chan Ying Chung, 2004, Solar Assisted Heat Pump Desalination. *Desalination*, vol. 168, pp 49 – 54
- Hermann, Michael, Joachim Koschikowski and Matthias Rommel, 2002, Corrosion-Free Solar Collectors for Thermally Driven Seawater Desalination. *Solar Energy*, Vol. 72, pp. 415-426
- Incropera, Frank P. and David P. DeWitt, 1985, *Fundamentals of Heat Transfer*. John Wiley and Sons
- Kalogirou, Soteris A., 2005, Seawater Desalination Using Renewable Energy Sources, *Progress in Energy and Combustion Science*, Vol. 31, pp 242–281
- Khan, Arshad Hassan, 1986, *Desalination Processes and Multistage Flash Distillation Practice*, Elsevier Science Publishers B.V.
- Kreider, Jan F., Charles J. Hoogendoorn, and Frank Keith, 1989, *Solar Design: Components, Systems, Economics*, Hemisphere Publishing Corporation
- Kudish, Avraham I., Efim G. Evseev, Gerd Walter and Thomas Priebe, 2003, Simulation Study on a Solar Desalination System Utilizing an Evaporator/Condenser Chamber. *Energy Conversion and Management*, vol. 44, pp 1653 – 1670
- Le Goff, Pierre, Jacqueline Le Goff and M. Razak Jeday, 1991, Development of A Rugged Design of A High Efficiency Multi Stage Solar-Still. *Desalination*, Vol. 82, pp. 153-163
- Marcovecchio, Marian G., Sergio F. Mussati, Pio A. Aguirre, Nicolas J. and Scenna, 2005, Optimization of Hybrid Desalination Processes Including Multi Stage Flash and Reverse Osmosis Systems. *Desalination*, vol. 182, pp 111 – 122
- Minasian, A.N. and A.A. Al-Karaghoul, 1992, Floating Vertical Solar Still for Desalination of Marsh Water. *Renewable Energy*, vol. 2 no 6, pp 631 – 635
- Nafey, A. Safwat, M.A. Mohamad, S.O. El-Helaby and M.A. Sharaf, 2007, Theoretical and Experimental Study of A Small Unit for Solar Desalination Using Flashing Process. *Energy Conversion and Management*, Vol. 48, pp. 528-538
- Rahim, Nabil Hussain A., 2001, Utilisation of New Technique to Improve the Efficiency of Horizontal Solar Desalination Still. *Desalination*, vol. 138, pp 121 – 128
- Rahim, N.H.A., 2003, New Method to Store Heat Energy in Horizontal Solar Desalination Still. *Renewable Energy*, vol. 28, pp 419 – 433

Rahman, KH. MD. Hafizur, 2002, A Study of Submerged Vertical Tube Evaporation In Multi Effect Desalination. M.Eng Thesis, National University of Singapore

Rajvanshi, Anil K., 1980, A Scheme for Large Scale Desalination of Sea Water by Solar Energy. Solar Energy, vol 24, pp 551 – 560

Reali, M., 1984, A Refrigerator Heat Pump Desalination Scheme for Fresh Water and Salt Recovery. Energy, vol. 9 no 7 pp 583-588

Rodriguez, Lourdes Garcia, Ana I. Palmero-Marrero and Carlos Gomez-Camacho, 2002, Comparison of Solar Thermal Technologies for Applications in Seawater Desalination. Desalination, Vol. 142, pp. 135-142

Sinha, S. and G.N. Tiwari, 1992, Thermal Evaluation of Concentrator Assisted Solar Distillation System. Heat Recovery Systems and CHP, vol. 12, no 6, pp 481 -488

Siqueiros, J. and F.A.Holland, 2000, Water Desalination Using Heat Pumps. Energy, vol. 25, pp 717-729

Slesarenko, V.V., 1999, Desalination Plant With Absorption Heat Pump for Power Station. Desalination, vol. 126, pp 281-285

Stein, Benjamin, John S. Reynolds, and William J. McGuinness, 1986, Mechanical and Electrical Equipment for Buildings 7th Edition, John Wiley and Sons

Wang, Xiaolin, and Kim Choon Ng, 2005, Experimental Investigation of an Adsorption Desalination Plant Using Low-temperature Waste Heat, Applied Thermal Engineering, vol. 25, pp 2780-2789

Wijeyesundera, N.E. and J.C. Ho, 1985, Comparison of Optimization Criteria for Solar Heating and Some Energy Conservation Measures. Energy Conversion Management, vol. 25, pp 331 – 337

APPENDIX A
EXPERIMENTAL DATA

Table A1. Experimental data of 12 December 2005

2005/12/12	Feed Inlet	Outlet Condenser Coil	Outlet Cooling Coil	Inlet Condenser Coil	Inlet Water Condenser	Water Condenser	Outlet Water Condenser	Outlet Expansion Valve
Time	101(C)	102(C)	103(C)	104(C)	105(C)	106(C)	107(C)	108(C)
10:56 AM	68.95	37.75	39.29	62.39	31.76	31.23	30.05	8.79
11:01 AM	70.26	38.34	43.02	63.15	31.74	31.09	30.05	5.46
11:06 AM	70.97	39.84	43.72	67.28	31.74	31.02	30.10	6.70
11:11 AM	70.04	40.88	44.03	70.87	31.94	31.53	30.12	5.13
11:16 AM	71.42	41.40	45.07	70.00	32.39	32.02	30.32	8.61
11:21 AM	74.46	42.05	45.45	70.46	32.61	32.01	30.47	5.83
11:26 AM	70.99	42.58	46.31	70.28	32.90	32.29	30.62	9.06
11:31 AM	71.54	42.42	30.80	68.71	32.35	31.65	30.64	10.66
11:36 AM	69.64	47.34	0.59	72.36	32.89	33.02	30.57	6.39
11:41 AM	71.64	50.05	14.01	66.24	32.65	32.00	30.85	10.18
11:46 AM	74.43	47.25	45.37	70.55	32.82	32.33	30.78	5.29
11:51 AM	73.92	44.59	46.65	70.75	33.04	32.52	30.90	5.05
11:56 AM	72.41	44.20	48.15	67.80	32.99	32.00	31.13	10.17
12:01 PM	73.81	44.80	50.44	64.29	33.14	32.47	31.18	10.15
12:06 PM	71.65	45.33	50.72	68.66	33.50	32.68	31.23	8.84
12:11 PM	73.73	45.65	50.47	72.56	33.38	32.48	31.28	9.04
12:16 PM	72.22	46.13	51.04	70.58	33.58	33.10	31.42	10.16
12:21 PM	75.19	47.20	45.93	69.61	33.99	33.53	31.54	8.31
12:26 PM	73.51	50.32	33.17	68.01	33.60	32.70	31.59	8.95
12:31 PM	72.72	52.33	42.63	68.48	33.73	33.76	31.73	10.45
12:36 PM	75.78	48.99	51.02	74.40	33.90	34.25	31.73	5.34
12:41 PM	75.16	46.56	51.70	68.82	33.56	32.58	31.83	8.58
12:46 PM	73.69	47.16	52.03	71.25	33.57	32.57	31.93	7.85
12:51 PM	75.46	46.88	51.32	74.30	33.54	33.52	31.95	5.65
12:56 PM	75.93	46.44	50.79	74.57	33.63	32.84	32.24	10.60

Table A1. Experimental data for 12 December 2005 (continued)

Inlet Solar Collector	Outlet Solar Collector	Inlet Compressor	Outlet Compressor	Outlet Compressor	Outlet Liquid Solar Collector	Inlet Solar Collector	let WaterIn Condenser	Inlet Compressor
109(C)	110(C)	111(C)	112(C)	113(VDC)	114(C)	115(VDC)	116(VDC)	117(VDC)
12.32	57.01	34.86	77.77	1.07	69.27	1.35	1.77	1.12
10.49	55.57	41.43	78.91	1.07	64.37	1.30	1.80	1.24
12.36	55.42	42.73	79.59	1.07	64.26	1.33	1.79	1.20
16.84	56.07	43.67	83.27	1.07	67.80	1.30	1.80	1.22
16.14	58.63	44.58	82.07	1.08	70.42	1.35	1.79	1.16
11.82	56.50	44.42	84.41	1.08	68.23	1.31	1.81	1.23
12.70	56.79	45.13	84.48	1.08	66.46	1.36	1.80	1.15
11.59	56.55	44.28	80.80	1.07	67.30	1.37	1.79	1.13
15.16	57.80	29.93	85.48	1.08	71.02	1.32	1.81	1.20
11.19	59.10	26.98	78.61	1.07	74.71	1.38	1.79	1.10
18.54	58.28	33.40	81.31	1.07	76.15	1.31	1.82	1.22
17.94	57.63	44.05	82.59	1.07	75.29	1.30	1.83	1.23
11.12	57.84	45.43	78.58	1.07	73.26	1.37	1.81	1.12
10.72	56.56	46.14	79.39	1.07	72.25	1.37	1.81	1.13
9.77	57.17	47.47	82.36	1.08	72.63	1.37	1.81	1.13
11.23	56.06	47.85	86.12	1.08	72.03	1.37	1.82	1.19
11.01	57.65	47.91	84.45	1.08	72.57	1.39	1.82	1.12
10.63	59.18	49.15	85.00	1.08	74.63	1.34	1.83	1.21
10.43	58.88	44.07	83.12	1.08	77.13	1.38	1.82	1.13
10.84	62.29	38.79	82.94	1.08	81.06	1.37	1.83	1.16
14.75	61.56	47.62	87.41	1.08	82.60	1.31	1.85	1.23
10.97	56.77	47.64	82.44	1.08	78.39	1.36	1.84	1.17
10.83	59.24	48.14	83.96	1.08	77.62	1.34	1.85	1.21
15.66	59.89	49.57	87.68	1.07	83.34	1.32	1.86	1.25
20.91	62.72	49.00	84.45	1.08	87.52	1.38	1.84	1.17

Table A1. Experimental data for 12 December 2005 (continued)

Solar Irradiation	Ambient Temperature	Inlet Cooling Coil	Coefficient of Performance	Efficiency of evaporator collector	Efficiency of liquid solar collector	Energy Input by Preheater
118(VDC)	119(C)	120(C)	COP	%	%	W
0.00	28.96	8.42	6.20	89.24	62.32	0.00
0.01	29.55	5.96	7.33	62.35	37.83	68.36
0.01	29.21	6.03	6.77	46.11	29.17	78.05
0.01	29.98	6.79	9.28	44.68	34.19	25.99
0.01	30.62	6.27	9.30	60.34	45.53	11.62
0.01	30.40	5.83	8.80	68.75	46.78	72.44
0.01	30.61	6.16	9.21	63.59	41.79	52.63
0.01	30.61	5.70	8.22	54.34	35.84	49.26
0.01	32.44	6.09	5.26	49.46	37.77	0.00
0.01	30.80	8.12	5.05	51.58	38.25	0.00
0.01	30.68	7.12	6.08	48.68	44.82	0.00
0.01	30.92	8.28	8.69	48.13	43.57	0.00
0.00	30.67	8.00	8.46	77.14	56.76	0.00
0.01	31.04	7.60	8.42	53.87	39.48	18.08
0.01	31.49	6.78	7.99	61.45	43.95	0.00
0.01	31.17	7.46	7.22	59.61	44.44	19.79
0.01	32.54	6.94	7.59	54.98	39.88	0.00
0.01	32.57	7.23	7.75	57.47	41.96	6.51
0.01	31.43	6.70	7.01	46.53	35.97	0.00
0.00	32.47	7.77	6.10	98.77	77.81	0.00
0.01	34.21	7.53	6.91	38.92	34.68	0.00
0.01	32.04	6.93	7.98	62.29	52.34	0.00
0.01	32.03	6.83	7.73	45.66	35.68	0.00
0.01	33.44	6.85	7.24	38.72	37.04	0.00
0.01	32.77	6.88	7.81	37.23	40.52	0.00

Table A2. Experimental data for 13 December 2005

2005/13/12	Feed Inlet	Outlet Condenser Coil	Outlet Cooling Coil	Inlet Condenser Coil	Inlet Water Condenser	Water Condenser	Outlet Water Condenser	Outlet Expansion Valve
Time	101(C)	102(C)	103(C)	104(C)	105(C)	106(C)	107(C)	108(C)
11:10 AM	70.85	34.96	34.37	58.85	27.90	28.15	32.21	5.39
11:15 AM	73.68	36.70	41.72	52.81	28.01	29.30	32.26	9.56
11:20 AM	76.21	39.52	43.16	49.24	28.19	29.47	32.15	9.75
11:25 AM	72.32	41.65	47.68	50.59	28.47	29.87	32.35	10.41
11:30 AM	73.76	43.35	49.21	53.11	28.70	30.87	32.31	10.13
11:35 AM	71.34	44.17	50.75	56.53	29.00	31.67	32.39	10.35
11:40 AM	72.84	44.66	51.48	62.95	29.27	31.93	32.46	10.13
11:45 AM	76.07	46.97	34.13	65.97	29.47	32.08	32.48	10.56
11:50 AM	72.32	49.29	42.83	65.40	29.56	32.15	32.51	10.32
11:55 AM	74.33	46.40	49.98	72.75	29.89	32.24	32.60	9.93
12:00 PM	71.73	45.72	51.85	66.79	29.80	32.27	32.69	10.34
12:05 PM	73.48	47.32	53.80	66.43	30.10	34.07	32.77	10.32
12:10 PM	73.26	46.73	53.22	68.65	30.28	33.50	32.75	9.98
12:15 PM	72.84	45.84	52.96	70.16	30.43	32.20	32.80	10.22
12:20 PM	75.95	45.78	52.62	70.52	30.63	32.16	32.90	7.35
12:25 PM	72.78	47.61	35.82	68.55	31.04	32.05	33.00	10.66
12:30 PM	75.77	51.03	8.14	71.26	31.11	32.74	33.02	9.89
12:35 PM	73.35	51.25	16.88	73.29	31.47	33.91	33.15	6.44
12:40 PM	77.57	49.25	50.44	67.60	31.87	32.74	33.40	5.48
12:45 PM	74.65	47.20	46.99	65.93	31.88	33.18	33.37	10.07
12:50 PM	73.51	48.01	44.35	66.28	32.08	32.91	33.48	10.16
12:55 PM	74.52	47.22	50.08	66.38	32.21	32.73	33.60	7.00
1:00 PM	72.62	47.71	48.00	65.13	32.21	32.07	33.60	10.21
1:05 PM	75.56	50.04	27.90	67.35	32.17	32.86	33.61	7.63
1:10 PM	74.44	50.79	43.97	68.98	32.41	34.12	33.75	9.43

Table A2. Experimental data for 13 December 2005 (continued)

Inlet Solar Collector	Outlet Solar Collector	Inlet Compressor	Outlet Compressor	Outlet Compressor	Outlet Liquid Solar Collector	Inlet Solar Collector	Inlet Water Condenser	Inlet Compressor
109(C)	110(C)	111(C)	112(C)	113(VDC)	114(C)	115(VDC)	116(VDC)	117(VDC)
18.98	46.42	22.53	69.41	1.07	68.19	1.30	1.84	1.15
10.03	47.12	32.82	66.65	1.07	65.22	1.35	1.83	1.10
10.83	47.65	35.63	63.70	1.06	64.85	1.36	1.82	1.07
10.83	48.73	37.62	71.44	1.07	64.84	1.38	1.83	1.11
10.68	48.77	39.13	73.41	1.07	64.47	1.37	1.83	1.10
10.77	49.01	40.52	75.97	1.07	64.06	1.37	1.83	1.11
10.82	48.81	43.01	80.99	1.07	63.64	1.38	1.84	1.15
11.08	48.93	41.04	81.27	1.07	63.72	1.38	1.84	1.14
10.73	49.19	39.19	82.09	1.07	64.24	1.38	1.84	1.13
13.63	49.67	44.36	84.39	1.07	64.64	1.38	1.85	1.14
10.93	49.40	44.83	82.46	1.07	64.84	1.38	1.85	1.15
10.68	50.19	45.61	83.20	1.07	64.86	1.38	1.85	1.15
11.09	49.62	46.53	84.61	1.07	64.60	1.34	1.87	1.25
12.51	49.30	46.00	84.66	1.07	64.87	1.38	1.86	1.15
11.34	48.86	46.65	86.61	1.07	65.30	1.34	1.88	1.25
11.37	49.68	44.03	83.03	1.07	65.87	1.39	1.86	1.14
13.54	50.20	30.88	83.90	1.07	67.57	1.39	1.86	1.11
17.00	50.22	24.87	84.24	1.07	69.31	1.33	1.89	1.24
11.51	50.75	31.53	80.98	1.07	69.76	1.31	1.89	1.24
10.74	50.90	42.54	77.67	1.07	68.85	1.38	1.87	1.12
10.63	50.72	39.54	79.49	1.07	67.88	1.38	1.87	1.14
12.29	50.78	41.09	83.14	1.07	68.35	1.33	1.89	1.23
10.98	51.60	43.92	79.45	1.07	69.51	1.39	1.88	1.15
9.65	51.53	40.23	81.81	1.07	70.86	1.34	1.89	1.21
10.37	52.40	37.11	82.02	1.07	70.90	1.38	1.88	1.14

Table A2. Experimental data for 13 December 2005 (continued)

Solar Irradiation	Ambient temperature	Inlet Cooling Coil	Coefficient of Performance	Efficiency of evaporator collector	Efficiency of liquid solar collector	Energy Input by Preheater
118(VDC)	119(C)	120(C)	COP	%	%	W
0.00409	28.98	6.38	4.65	62.09	57.22	30.93
0.00411	29.45	8.59	5.76	83.38	52.51	98.25
0.00416	29.50	6.58	5.62	81.81	51.34	131.95
0.00408	30.01	7.55	7.50	85.95	52.35	86.85
0.00411	29.46	9.16	7.67	85.63	51.33	107.94
0.00398	30.76	7.21	7.71	88.84	52.41	84.56
0.00392	29.95	8.13	8.57	89.60	52.56	106.91
0.00396	29.67	5.16	7.42	88.42	52.17	143.56
0.00401	29.93	6.26	6.59	88.60	52.24	93.92
0.00376	29.70	6.36	8.04	88.65	56.38	112.64
0.00402	29.92	5.36	8.67	88.49	53.06	80.05
0.00399	31.21	7.00	9.32	91.66	53.55	100.16
0.00402	30.39	7.33	8.90	88.58	52.68	100.68
0.00428	29.84	8.33	7.31	79.55	49.91	92.58
0.00419	29.35	8.43	7.04	82.81	51.60	123.76
0.00456	29.82	8.24	7.21	77.68	48.15	80.31
0.00503	30.17	8.59	5.07	67.41	45.70	95.31
0.00489	31.49	7.56	4.47	62.98	49.25	46.99
0.00434	30.38	8.37	5.44	83.60	56.05	90.70
0.00423	30.97	8.55	8.12	87.88	56.25	67.49
0.00457	30.72	7.52	6.96	81.12	50.72	65.38
0.00479	30.53	6.45	6.57	74.36	49.00	71.80
0.00489	29.77	7.54	8.01	76.88	49.46	36.19
0.00481	30.39	9.20	6.65	80.56	52.01	54.60
0.00488	31.11	9.62	6.07	79.83	51.37	41.17

Table A3. Experimental data for 23 January 2006

2005/23/1	Feed Inlet	Outlet Condenser Coil	Outlet Cooling Coil	Inlet Condenser Coil	Inlet Water Condenser	Water Condenser	Outlet Water Condenser	Outlet Expansion Valve
Time	101(C)	102(C)	103(C)	104(C)	105(C)	106(C)	107(C)	108(C)
12:07 PM	67.49	46.92	54.24	55.96	28.47	29.71	29.97	9.48
12:13 PM	65.60	48.98	24.63	66.80	28.72	29.53	29.92	4.25
12:19 PM	72.10	48.68	51.95	55.64	29.03	30.46	30.20	9.64
12:25 PM	69.92	47.73	55.02	54.96	29.39	30.65	30.29	8.88
12:31 PM	69.68	47.75	55.84	57.26	29.62	30.39	30.29	9.72
12:37 PM	69.98	48.42	54.67	64.25	29.90	30.93	30.11	4.19
12:43 PM	71.21	47.84	55.32	63.52	30.40	32.00	30.46	9.01
12:49 PM	68.20	48.99	56.39	62.88	30.97	31.91	30.58	9.46
12:55 PM	72.42	50.98	51.89	61.90	31.04	31.85	30.71	8.88
1:01 PM	69.72	48.91	54.70	68.65	30.98	31.00	30.51	5.15
1:07 PM	68.34	48.68	54.99	66.42	31.14	32.31	30.69	3.44
1:13 PM	69.86	47.79	55.79	61.04	31.12	30.47	30.81	7.39
1:19 PM	69.95	48.12	54.67	67.83	31.17	31.35	30.83	7.44
1:25 PM	69.12	48.24	56.43	62.93	31.31	31.05	31.03	9.94
1:31 PM	73.84	49.43	57.02	60.77	31.49	32.90	31.11	9.21
1:37 PM	69.47	49.44	41.00	70.27	31.69	32.20	30.98	6.93
1:43 PM	68.68	50.50	53.04	61.03	31.24	31.55	31.20	9.74
1:49 PM	73.13	49.12	56.30	60.46	31.34	32.46	31.29	8.49
1:55 PM	68.08	49.21	56.84	61.44	31.29	32.87	31.33	9.91
2:01 PM	72.18	49.14	55.30	67.85	31.35	32.52	31.10	5.05
2:07 PM	68.62	48.11	56.11	65.33	31.35	32.18	31.50	9.67
2:13 PM	75.88	48.28	54.75	68.58	31.34	32.54	31.31	6.30

Table A3. Experimental data for 23 January 2006 (continued)

Inlet Solar Collector	Outlet Solar Collector	Inlet Compressor	Outlet Compressor	Outlet Compressor	Outlet Liquid Solar Collector	Inlet Solar collector/Coil	Inlet Water Condenser	Inlet Compressor
109(C)	110(C)	111(C)	112(C)	113(VDC)	114(C)	115(VDC)	116(VDC)	117(VDC)
10.69	36.99	37.95	72.31	1.08	46.59	1.40	1.77	1.08
17.08	37.51	36.76	78.86	1.10	47.96	1.31	1.80	1.20
10.77	39.18	33.67	71.73	1.08	49.27	1.39	1.78	1.09
10.43	40.90	37.13	72.33	1.12	51.34	1.39	1.78	1.10
10.64	41.12	40.25	73.96	1.08	51.91	1.39	1.78	1.11
13.64	41.82	45.94	80.13	1.08	53.27	1.31	1.81	1.22
10.26	44.90	44.79	77.48	1.08	56.89	1.39	1.80	1.15
10.88	47.23	45.71	78.59	1.09	58.03	1.40	1.80	1.13
10.66	47.87	45.46	78.86	1.07	59.10	1.39	1.80	1.16
18.79	46.22	48.43	81.20	1.08	58.28	1.33	1.82	1.22
16.41	46.00	47.22	79.22	1.08	57.37	1.34	1.80	1.16
10.52	45.62	44.68	76.54	1.07	56.78	1.33	1.82	1.23
18.11	45.57	47.14	79.75	1.16	55.64	1.34	1.81	1.19
11.31	45.21	44.54	76.99	1.12	54.92	1.40	1.80	1.13
10.53	46.34	44.66	77.21	1.38	56.41	1.39	1.81	1.14
18.83	46.60	47.33	82.24	1.10	59.23	1.35	1.83	1.21
10.89	44.87	40.03	75.70	1.08	57.60	1.40	1.81	1.12
10.23	45.00	42.61	76.60	1.08	56.00	1.37	1.82	1.15
10.56	45.02	44.42	77.73	1.07	55.72	1.39	1.82	1.15
15.63	44.45	47.04	82.26	1.07	57.11	1.33	1.84	1.23
11.39	44.30	45.28	78.94	1.06	56.79	1.39	1.82	1.15
18.58	44.15	47.77	81.33	1.05	58.24	1.36	1.84	1.21

Table A3. Experimental data for 23 January 2006 (continued)

Solar Irradiation	Ambient Temperature	Inlet Cooling Coil	Coefficient of Performance	Efficiency of evaporator collector	Efficiency of liquid solar collector	Energy Input by Preheater
118(VDC)	119(C)	120(C)	COP	%	%	W
0.0030	28.38	28.42	8.26	96.82	34.05	242.77
0.0031	28.26	-1.03	6.53	73.14	35.83	204.98
0.0031	29.06	21.86	7.27	100.19	37.79	265.28
0.0034	28.75	25.47	8.00	99.92	38.86	215.83
0.0031	28.84	25.36	8.46	107.08	42.72	206.44
0.0045	29.39	1.22	8.36	69.13	31.65	194.15
0.0043	30.32	12.73	8.80	88.94	38.20	166.43
0.0039	30.10	11.57	8.73	104.16	44.37	118.20
0.0041	29.88	9.96	8.57	101.10	43.66	154.85
0.0040	30.09	1.18	8.79	75.87	43.16	132.94
0.0038	30.17	7.78	9.03	87.09	37.84	175.05
0.0035	28.95	13.29	9.33	110.32	46.56	151.98
0.0036	30.13	4.89	9.06	84.23	43.44	166.28
0.0035	28.96	16.36	9.10	108.77	44.24	164.94
0.0045	30.93	21.90	9.06	87.47	35.67	202.52
0.0038	29.74	0.16	8.34	80.33	46.65	119.02
0.0034	29.47	11.70	8.07	109.70	49.29	128.73
0.0037	29.97	22.41	8.57	103.22	42.72	198.98
0.0037	30.69	21.75	8.79	102.07	42.16	143.66
0.0039	30.14	2.48	8.24	82.67	43.01	175.11
0.0042	30.14	8.90	8.67	87.65	39.51	137.40
0.0040	31.46	0.38	8.72	70.50	43.05	205.01

APPENDIX B

COMPRESSOR PRICE LIST
AND
AIR CONDITIONER COOLING CAPACITY

A short list of compressor prices and commercial air conditioner cooling capacity is shown in this section. For a full range of price and air conditioner capacity, please refer to www.thermacom.com and www.daikin.com.sg, respectively.

Table B1. Compressor prices (www.thermacom.com)


Make/Model	Equivalent	Weight(kg)	Trade	Euro
Bitzer				
				
Semi Hermetic				
2HL1.2	BHS 171	50	£400	€590
2GL2.2	BHS 191	50	£400	€590
2FL2.2	BHS 231	70	£400	€590
2DL2.2	BHS 351	50	£425	€595
2DL3.2	BHS 491	50	£425	€595
2EL2.2		50	£425	€595
2Us.2	BHS 502	70	£475	€665
2Q4.2	BHS 592	70	£475	€665
2Us.2	BHS 802	70	£500	€700
2Q6.2	BHS 962	90	£500	€700
2Ns.2		90	£500	€700
4V6.2	BHS 902	85	£725	€1,015
4Z5.2	BHS 752	140	£700	€980
4Z8.2	BHS 1252	150	£750	€1,050
4T8.2	BHS 1102	150	£750	€1,050
4P10.2	BHS 1282	150	£795	€1,113
4V10.2	BHS 1452	150	£795	€1,113
4N12.2	BHS 1522	150	£1,025	€1,435
4T12.2	BHS 1702	150	£1,025	€1,435
4P15.2	BHS 2022	150	£1,050	€1,470
4N20.2	BHS 2402	150	£1,075	€1,505
4M10.2		180	£1,075	€1,505
4J13.2		180	£1,200	€1,680
4H15.2		180	£1,225	€1,715
4M20.2		180	£1,200	€1,680
4J22.2		180	£1,225	€1,715
4G20.2		180	£1,285	€1,790
4H25.2	Trane CRHZ 200	180	£1,350	€1,890
4G30.2	Trane CRHZ 250	180	£1,375	€1,903
6M20.2		200	£1,400	€1,925
6J22.2		200	£1,400	€1,925
6H25.2		200	£1,550	€2,170
6G25.2		200	£1,550	€2,170
6M30.2		220	£1,550	€2,170
6G30.2		220	£1,750	€2,450
6J33.2		220	£1,700	€2,380
6H35.2	Trane CRHZ 300	220	£1,775	€2,485
6G40.2		220	£1,825	€2,555
6F40.2		220	£1,975	€2,785
6F50.2		240	£2,075	€2,905
6E60.2		400	£2,450	€3,430
6D70.2		450	£2,650	€3,710

Table B2. Cooling capacity of air conditioners (www.daikin.com.sg)

Air Conditioners up to 12 kW / Air Cooled / Split / Reverse Cycle					
Refrigerant R410A					
Outdoor	Indoor unit	Cooling Capacity (KW)	Cooling power input (KW)	EER	Class EER
RN20C	FTN20C	2	0.62	3.23	A
RKH20C	FTKS20C	2	0.62	3.23	A
ARKH20C	ATKS20C	2	0.62	3.23	A
ARKS35B	ATKS20C	2	0.5	4	A
RN25C	FTN25C	2.25	0.7	3.21	A
RKH25C	FTKS25C	2.25	0.7	3.21	A
ARKH25C	ATKS25C	2.25	0.7	3.21	A
RS20B	FTS20B	2.5	0.89	2.81	C
RKS25B	FTKS25B	2.5	0.7	3.57	A
RK25B	FTK25B	2.5	0.89	2.81	C
ARK25B	ATK25B	2.5	0.89	2.81	C
ARKS25B	ATKS25B	2.5	0.7	3.57	A

APPENDIX C
SAMPLE CALCULATION

An example of a manual calculation to find a payback period for a given economic parameters is presented here. The parameters taken into account, and its values, are:

$$C_F = \text{S\$ } 0.06 / \text{ MJ}$$

$$C_C = \text{S\$ } 250 / \text{ m}^2$$

$$n = 20 \text{ years}$$

$$C_M + C_O = 0.1 * C_S$$

$$e = 0.03$$

$$Q_S = 1.97 \times 10^5 \text{ MJ}$$

$$i = 0.07$$

$$C_I = \text{S\$ } 7,500$$

$$j = 0.014$$

$$A = 40 \text{ m}^2$$

To find the payback period, first we must first find the effective discount rate (i'), capital recovery factor (C_{RF}), and collector area related cost (C_S).

$$i' = \left(\frac{i - j}{1 + j} \right) = 0.055$$

$$C_{RF}(i', n) = \left\langle \left\{ \frac{1}{i} \left[1 - \left(\frac{1}{1 + i} \right)^n \right] \right\}^{-1} \right\rangle = 0.084$$

$$C_S = C_D A + C_I = 17,500$$

Then, we can find the x_{pp} :

$$x_{pp} = \frac{C_S + \frac{(C_M + C_O)}{C_{RF}(i', n)}}{Q_S C_F} = 3.24$$

$$n_p = \frac{\ln[1 - (i - e)x_{pp}]}{\ln\left(\frac{1 + e}{1 + i}\right)} = 3.6$$

Thus, the payback period of the system is 3.6 years.